European Commission

JRC TECHNICAL REPORTS

Scenarios of Nutrient Management for Cleaner Seas:

Application on the Mediterranean

Towards a global water energy food nexus assessment

Anna Malago'
Fayçal Bouraoui
Iacopo Ferrario
Bruna Grizzetti

2016

Joint Research Centre

EUR 28424 EN

JRC Science Hub
https://ec.europa.eu/jrc

JRC105318

EUR 28424 EN

PDF	ISBN 978-92-79-65145-8	ISSN 1831-9424	doi:10.2760/51281
Print	ISBN 978-92-79-65146-5	ISSN 1018-5593	doi:10.2760/443241

Luxembourg: Publications Office of the European Union, 2016

How to cite this report: Malago' A., Bouraoui F., Ferrario I., Grizzetti B.; *Scenarios of Nutrient Management for Cleaner Seas: Application on the Mediterranean*; EUR 28424; Luxembourg (Luxembourg): Publications Office of the European Union; doi:10.2760/51281

Table of contents

Acknowledgments 4
Abstract 5
1. Introduction 6
2. Modelling approach 8
3. Model parameterization 10
3.1 Landcover/Landuse 10
3.2 Crop data 12
3.2.1 Crop uptake 12
3.2.2 Crop residue 12
3.2.3 Biological nitrogen fixation 12
3.3 Mineral and manure fertilizers 15
3.4 Human waste and industrial discharge 20
3.4.1 Domestic nutrient emission 20
3.4.2 Industrial emissions 23
3.4.3 Phosphorus emissions from detergents 23
3.5 The global spatial distribution of point sources and scattered dwelling 24
3.6 Atmospheric deposition 29
3.7 Hydrography and routing 30
4. Modelling results 32
4.1 Calibration and evaluation of model performance 32
4.2 Scenarios building 35
4.3 Results and discussion 35
5. Conclusions 40
6. References 41
List of figures 44
List of tables 46

Acknowledgments

We thank all the colleagues that contributed with their work to provide insightful global input data that were used in this study. We specially thank Ad De Roo who has shared meteorological data and the water discharge at different spatial and temporal scale. We are also indebted to Olga Vigiak for providing an R-version of the GREEN model.

Abstract

The Mediterranean Sea is a semi-closed sea connected with the open sea through the Strait of Gibraltar. Due to the circulation pattern and the long residence time, the Mediterranean Sea is a sensitive environment to eutrophication pressures and it is put at risk from direct and indirect impacts of human based activities. In this study, a new version of the model GREEN, originally developed for estimating nutrient loads from diffuse and points sources in Europe, was used based on a grid cell discretization (GREEN-Rgrid). The spatial resolution is 5 arc-minute resolution (9.2 km at the equator) and the model input consists of the latest and best available global data. The total nitrogen (TN) loads of year 2005 were successfully calibrated and evaluated respectively using 23 monitoring points. This baseline (BASE) was then compared with two different scenarios: S1, a scenario of agricultural sources reduction that consists in reducing the nitrogen surplus by 50%; and S2, a scenario that consists in upgrading all wastewater treatment plants efficiency to tertiary treatment. The S1 scenario resulted most effective than S2 in reducing the total nitrogen loads and specific loads in the Mediterranean subbasins. These results are not intended to be exhaustive, but were developed to give practical examples of what can be further achieved using the GRID-Rgrid model combined with global data.

1. Introduction

The Mediterranean is at the crossroad between three continents and different civilizations. Lately, the Mediterranean Sea has become the bridge for human crossing between the richer Southern European countries and the southern part of the Mediterranean countries affected by years of economic, social and political problems.

The Mediterranean is a semi-closed sea put at risk from direct and indirect impacts of human based activities despite the numerous international, regional and sub-regional initiatives that are in place for protecting the Mediterranean Sea. The Convention for the Protection of the Mediterranean Sea against Pollution was signed on 16 February 1976 in Barcelona. It was amended and renamed the Convention for the Protection of the Marine Environment and the Coastal Region of the Mediterranean, often called the Barcelona Convention. The 22 contracting parties including 21 countries and the European Union have adopted seven protocols including the Protocol for the Protection of the Mediterranean Sea against Pollution from Land-Based Sources and Activities that entered into force on 11 May 2008. The UNEP-MAP acts as the Secretariat of the Barcelona convention and its protocols. The "Horizon 2020 Initiative" of the European Union aims to de-pollute the Mediterranean by the year 2020 by tackling the sources of pollution that account for around 80% of the overall pollution of the Mediterranean Sea: municipal waste, urban waste water and industrial pollution. Horizon 2020 was endorsed during the Environment Ministerial Conference held in Cairo in November 2006 and is one of the key initiatives endorsed by the Union for the Mediterranean (UfM) since its launch in Paris in 2008.

Despite all these efforts, the Mediterranean region is experiencing a large stress on its water resources due to a combination of effects ranging from climate change to anthropogenic pressures due to an increasing water demand for domestic and industrial use, expansion of irrigated areas and tourism activities (Benoit and Comeau, 2005; Oron, 2003; Lacirignola et al., 2014). This stress is expected to increase due to a galloping urbanisation, industrialization, improved standard of living and population growth. However, water is a finite resource and a better management across sectors, across policy linked to water, energy, food and environment is required in view of achieving water security for the actual and future generations.

Some efforts were done in estimating water and nutrient fluxes into the sea. Strobl et al. (2013) used ArcView Generalized Watershed Loading Function Model (AVGWLF) to all coastal-adjacent catchments of the Mediterranean Sea to quantify water and nutrient loads into the Seas. However, this approach does not explicitly consider the spatial source of nutrients. Ludwig et al. (2009) used statistical regressions to estimate water and nutrient fluxes for year 2000 (and previous years), however without considering the major pressures impacting nutrient losses. Based on the global scale model IMAGE, Ludwig et al. (2010) estimated a spatially explicit water and nutrient budget for year 2000 at 0.5 deg (55 km at the equator) resolution. Another application including the Mediterranean is that of GLOBALNEWS where water and nutrients are explicitly estimated at a 0.5 deg resolution (Beusen et al., 2016).

The aim of this project is to quantify the loads of nutrients entering all seas at high spatial resolution (5 arc-minute resolution, 9.2 km at the equator) using the latest and best available global data in combination with the Green model (Grizzetti et al., 2012). The first objective is to quantify spatially the pressures coming from human activities that impact nutrient release in water bodies focusing specifically on agriculture, industrial activities and domestic water release for year 2005. The second part of the project is dedicated to the adjustments and modifications that were made to the original GREEN model for use at global scale. The third part of the study is focusing on a specific application on the Mediterranean Sea where the GREEN model is calibrated and evaluated, and then used to assess the impact of two nutrient management alternative scenarios for achieving a cleaner Mediterranean Sea.

The innovative aspects of the research is the use of newly released global data concerning crop distribution and crop yield throughout the world, the use of high resolution global climate data, high resolution population data used to discriminate between urban and rural settlements. In addition most of the global nutrient load assessments focus usually on year 2000 as baseline, however, human population growth and associated activities are changing rapidly and year 2000 is no longer representative of the actual situation. In this study we used year 2005 and in the near future we will update the agriculture pressure with year 2010 as soon as the new data is released.

2. Modelling approach

The modelling approach is based on that of GREEN (Grizzetti et al., 2012). GREEN is a conceptual statistical regression model that links nitrogen and phosphorus inputs to water quality measurements. GREEN considers two different sources of nutrients, which include applied fertilisers, atmospheric deposition, and scattered dwellings and point sources, that include, discharges from sewers, wastewater treatment plants and industries.

Diffuses sources transit first through the soil unsaturated and satured zones before reaching a stream and consequently undergo a preliminary reduction in the soil profile due mostly to the denitrification and storage processes. Once into the stream or water bodies these nutrients are subject to a second reduction due to algae growth and atmospheric losses. Point sources of nitrogen and phosphorus are only retained in streams and lakes. A routing structure is used to establish the emitting-receiving sub-basins relationship, where the up-stream nutrient load is added as an additional point source to the receiving down-stream sub-basin.

The original model structure requires the calibration of only two parameters one related to the annual rainfall driving the basin (saturated and unsaturated soil) retention, the second to the river length controlling the stream retention. The original model was formulated as follows:

Equation 1 $$L = \left[DS\ \alpha_P f(R) + (PS + UL)\right] \alpha_R f(L, RES\_T)$$

where L is the annual nutrient load (tons/year), DS is the sum of diffuse source within the basin (tons/year), PS are all the point sources emitted in the basin, UL is the upstream loads (tons/year), f is a reduction function which depends on the annual rainfall R(mm) for the retention taking place in the basin (including plant uptake, volatilization, denitrification) , and on the river length (L) and lake residence time (RES_T) for the water retention (including nutrient uptake, settling, denitrification), α_P is the basin retention parameter, and α_R is the water body retention parameter.

The calibration approach consists in determining the two parameters α_P and α_R. A good evaluation of the two parameters requires an extended monitoring dataset. The approach can be used for any determinant either dissolved, particulate, or combined such as for total N and P. Addition details about the original model procedure are found in Grizzetti et al. (2012).

The GREEN model was rewritten and modified in R programing language in order to provide a more flexible instrument increasing the reproducibility of the modelling approach (hereafters GREEN-Rgrid). There are several reasons for choosing R: first, R is by far the most popular language in data science; second, the R community is constantly adding new packages and features; and in addition, it allows integrating the power of Geographical Information Systems (GIS) extending R with classes and methods for spatial data (Pebesma and Bivand, 2005; Bivand et al.,2013).

The GREEN-Rgrid code was modified integrating a landscape routing model to simulate nutrient fluxes of total nitrogen and total phosphorous across discretized routing units. The spatial resolution and discretization depends on the purpose of the modelling and the user can use a grid cell size from finer to coarse resolution. The grid-based approach was adopted to adapt to the readily available global raster data that can be easily incorporated as model inputs providing a more homogeneous nutrient assessment between different areas of the world.

The approach was modified by considering as diffuse source DS the gross nutrient balance from agricultural land that is computed as the difference between the inputs (fertilizer application, fixation, and atmospheric deposition) and the output (crop nutrient uptake). A positive gross nutrient balance indicates the potential grid cells with higher risk of pollution, while a negative gross nutrient designates soils which with time may lose their fertility (Grizzetti et al., 2008). In the latter case, the diffuse sources from agriculture were set to zero in the model. Another important change respect to the original GREEN model concerns the calculation background losses that correspond mostly to losses from natural areas including forests. In the original model, a factor of 0.38 was considered to calculate the fraction of atmospheric deposition from forest areas that returns to the streams. In GREEN-Rgrid a new parameter α_N substitute the factor 0.38 and was calibrated together of the two parameters α_P and α_R. The new mass balance of the model can thus be formulated as:

Equation 2 $$L = \left[DS\ \alpha_P f(R) + ATM_{FOR}\ \alpha_N + \alpha_P\ (PS + UL)\right] \alpha_R f(L, RES\_T)$$

where ATM_{FOR} is the atmospheric deposition on forested and natural areas. The calibration of the three parameters was performed designing a Lating Hypercube approach using the FME package in R (Soetaert and Petzoldt, 2010). We performed 100 simulations changing the parameter α_P in the range 1-10, α_R in the range 0.001-0.05 and α_N in the range 0.2 and 0.6. The best simulation was chosen as the one maximizing the Nash Sutcliffe coefficient (Nash and Sutcliffe, 1970) computed using the observed and simulated annual loads for year 2005.

In the following sections, we illustrate how total nitrogen and total phosphorous inputs and outputs were evaluated globally describing both their estimation and spatial distributions.

3. Model parameterization

3.1 Landcover/Landuse

The GLOBCOVER 2009 map (Arino et al., 2008) with spatial grid resolution of about 200-300 m was used to define 10 classes of landcover: arable land (ARAB), fodder grazing (FODG), grass land (GRAS), forest (FRST), shrub (SHRU), bare (BARE), urban area (URHD), water (WATR), sea (WSEA) and snow (SNOW). These classes were summarized in grid cells of 5 minutes at global scale. The aggregated values at country level were checked against the FAOSTAT national statistics and when necessary the various classes were adjusted. In particular, the forest, grass land and snow were the classes that required the major adjustments as often the classes are a mixture of different landcover classes. The extent of the class arable land, ARAB, was fixed using the information of used agricultural land reported in the Spatial Production Allocation Model (SPAM) at 5 minutes of resolution. The class FODG was then obtained as the difference between the aggregated classes chosen as representative of the arable land and the agricultural land of SPAM.

For Serbia and Montenegro the arable land from SPAM were underestimated and was adjusted using the FAOSTAT information. The spatial distributions of ARAB, FRST and GRAS at global scale are shown in Figures 1, 2, and 3.

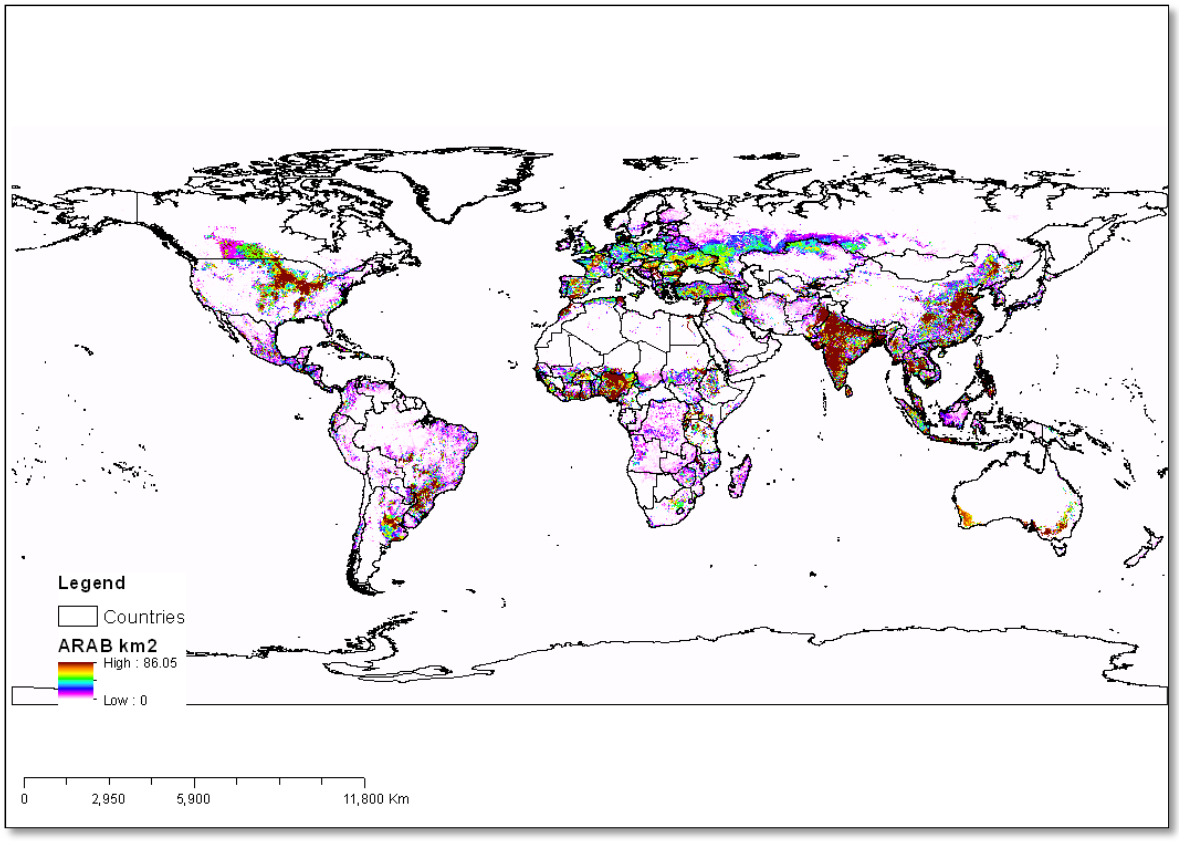

Figure 1. Global spatial distribution of arable land extent (km^2) at 5 minutes grid cell resolution.

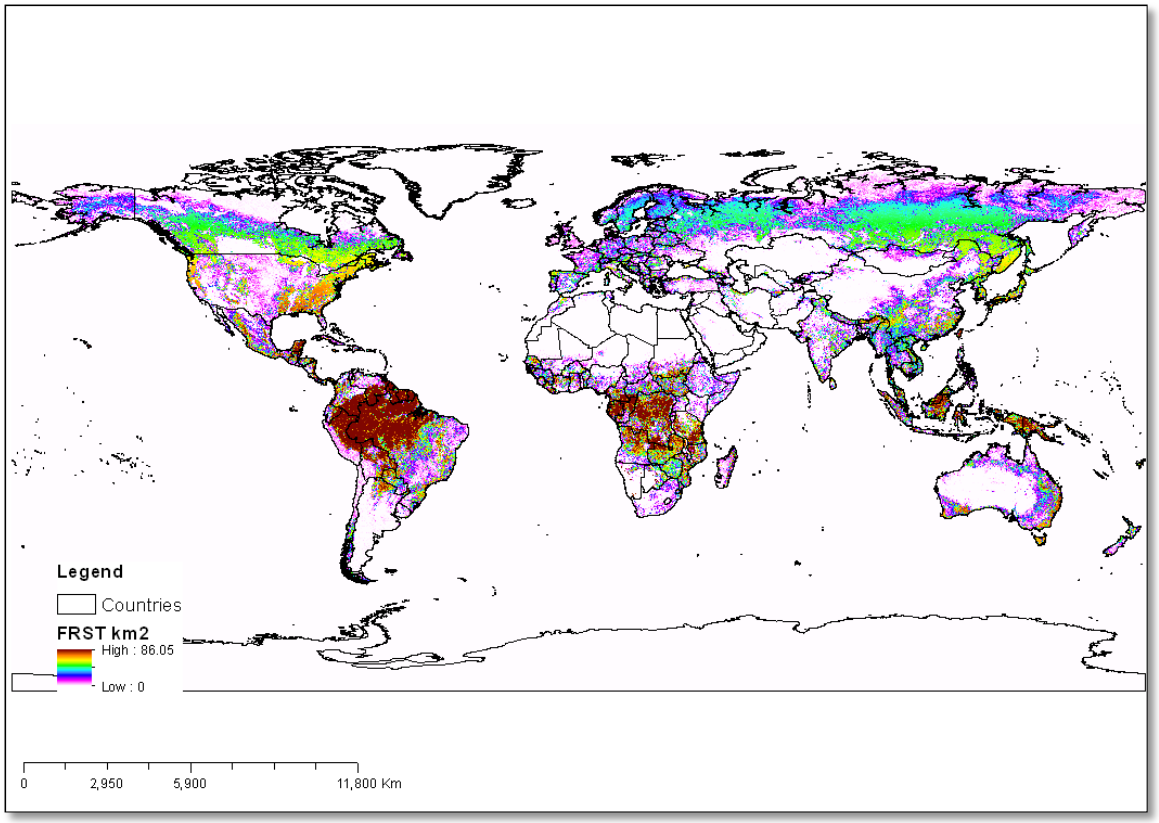

Figure 2. Global spatial distribution of forest extent (km^2) at 5 minutes grid cell resolution.

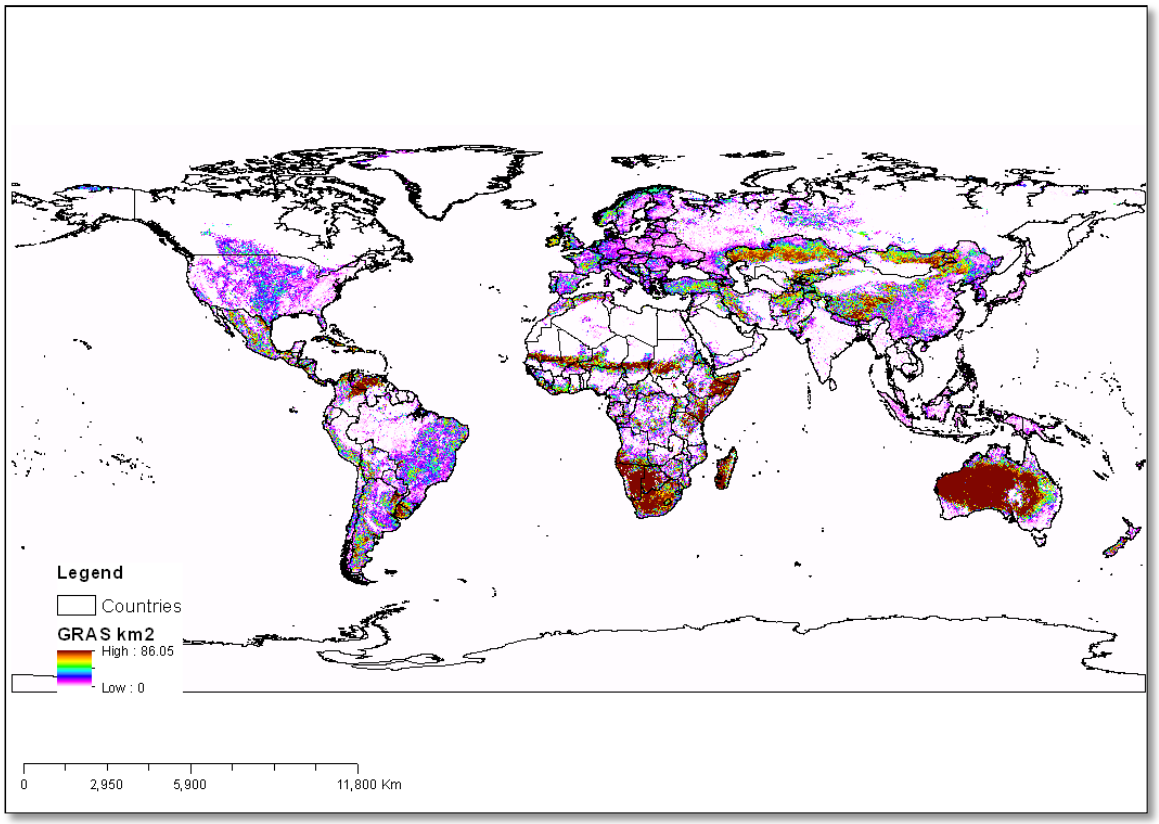

Figure 3. Global spatial distribution of grass land (km^2) at 5 minutes grid cell resolution.

3.2 Crop data

The basic data to characterize pressure coming from agriculture is the output of the Spatial Production Allocation Model (SPAM; You et al., 2014). The model was developed by IFPRI to generate crop areas, crop yield at a 5 arc-minute resolution using all relevant spatial explicit background information including "national and sub-national crop production statistics, satellite data on land cover, maps of irrigated areas, biophysical crop suitability assessments, population density, secondary data on irrigation and rain fed production systems, cropping intensity, and crop prices" (You et al., 2014). More specifically it provides for 42 crops and four levels of intensifications the physical area where a crop is grown, the harvest area for a specific crop to consider multiple-harvest in a specific year, the yield and the production (product of yield and harvest area). Data are provided for year 2005 (average of 3 years centred on 2005) for four production systems including irrigated high inputs production, rainfed high inputs production, rainfed low inputs production, rainfed subsistence production (You et al., 2014). The crops are described in Table1.

The SPAM yields expressed in terms of fresh weights were converted into dry weights using conversion coefficients of moisture contents of crops from the EPIC model (Williams, 1995) and literature (i.e. Milbrant, 2005). The distribution between above ground biomass and root was calculated using the Harvest Index taken from the SWAT crop database (Neitsh et al., 2010). This conversion was necessary to calculate the nutrient crop uptake and the crops residues. The nitrogen and phosphorous contents of each crop were retrieved from the SWAT model database (Neitsh et al., 2010) and are presented in Table1. The wet yields of FODG were retrieved from FAOSTAT at country level and then converted in dry yields using the moisture content in Table1.

3.2.1 Crop uptake

The nitrogen and phosphorous uptake was obtained by multiplying the crop dry yield from SPAM by the corresponding crop coefficients listed in Table 1. This resulted in a raster map for each crop and each production system. Figure 4 shows the wheat nitrogen uptake at global scale. The FODG crop nitrogen and phosphorus uptake and residue and biological fixation at country level were distributed at grid level based on the distribution of animals (see next sections).

3.2.2 Crop residue

The crop residues were calculated by multiplying the dry yields with a "residue to product ratio" (RPR) calculated from the harvest index HI:

Equation 3 $$RPR = \left[1 - HI\right] / HI$$

Figure 5 shows the raster map of crop soybean residue at global scale.

3.2.3 Biological nitrogen fixation

The nitrogen fixation for each crop was calculated based on the harvest area of each crop and then aggregated at country level. The total nitrogen fixation at country level was then distributed in each grid cell inside the country based on the spatial distribution of crop uptake. It is noteworthy that for all crops a soil organism fixation of 4 kg/ha was considered (Table1). Figure 6 shows the raster map of nitrogen fixation for all crops obtained at global scale. The same procedure was adopted to distribute at grid cell level the nitrogen fixation for FODG.

Table 1. SPAM crops and related coefficients used in this work.

code	description	CNYLD[1]	CPYLD[2]	HVSTI[3]	RPR[4]	FIX kg/ha[5]	MC (%)[6]
acof	arabica coffee	0.0015	0.0003	0.15	0	4	60
bana	banana	0.0064	0.0008	0.44	0	4	74
barl	barley	0.021	0.0017	0.54	0.851852	4	12
bean	bean	0.037	0.0021	0.45	1.222222	40	12
cass	cassava	0.0097	0.001	0.6	0.666667	4	80
chic	chickpea	0.0427	0.0048	0.42	1.380952	60	12
cnut	coconut	0.0015	0.0003	0.56	0	4	45
coco	cocoa	0.0015	0.0003	0.15	0	4	60
cott	cotton	0.014	0.002	0.5	1	4	1
cowp	cowpea	0.0427	0.0048	0.42	1.380952	60	12
grou	groundnut	0.0505	0.004	0.4	1.5	80	6
lent	lentil	0.0506	0.0051	0.61	0.639344	60	12
maiz	maize	0.014	0.0016	0.5	1	4	15
ocer	other cereals	0.0316	0.0057	0.42	1.380952	4	10
ofib	other fibre crops	0.04	0.0033	0.54	0.851852	4	12
oilp	oilpalm	0.0019	0.0004	0.18	0	4	30
ooil	other oil crops	0.0015	0.0003	0.05	0	4	60
opul	other pulses	0.037	0.0021	0.45	1.222222	60	12
orts	other roots	0.0097	0.001	0.6	0.666667	4	80
pige	pigeonpea	0.0427	0.0048	0.42	1.380952	60	12
plnt	plantain	0.0064	0.0008	0.44	0	4	70
pmil	pearl millet	0.02	0.0028	0.25	3	4	12
pota	potato	0.0246	0.0023	0.95	0.052632	4	80
rape	rapeseed	0.0234	0.0033	0.25	3	4	8.5
rcof	robusta coffe	0.0015	0.0003	0.15	0	4	60
rice	rice	0.0136	0.0013	0.5	1	25	14
sesa	sesameseed	0.0019	0.0004	0.18	0	4	30
smil	small millet	0.02	0.0028	0.25	3	4	12
sorg	sorghum	0.0199	0.0032	0.9	0.111111	4	10
soyb	soybean	0.065	0.0091	0.31	2.225806	80	13
sugb	sugarbeet	0.013	0.002	2	0	4	80
sugc	sugarcane	0.0069	0.0017	0.5	1	4	77
sunf	sunflower	0.0454	0.0074	0.3	2.333333	4	6
swpo	sweet potato	0.0097	0.001	0.6	0.666667	4	80
teas	tea	0.0015	0.0003	0.15	0	4	75
temf	temperate fruit	0.0019	0.0004	0.1	0	4	84
toba	tobacco	0.014	0.0016	0.55	0.818182	4	10
trof	tropical fruit	0.0019	0.0004	0.14	0	4	87
vege	vegetables	0.0259	0.0031	0.8	0.25	4	93
whea	wheat	0.0234	0.0033	0.42	1.380952	4	12
yams	yams	0.0097	0.001	0.6	0.666667	4	80
FODG	fodder crop and grazing	0.01	0.002	0.9	0.111111	65	73

[1] nitrogen content of crop (kg N/kg yield), [2] phosphorus content of crop (kg P/kg yield), [3] harvest index, [4] residue coefficient, [5] specific nitrogen fixation (kg N/ha) [6] moisture content (%).

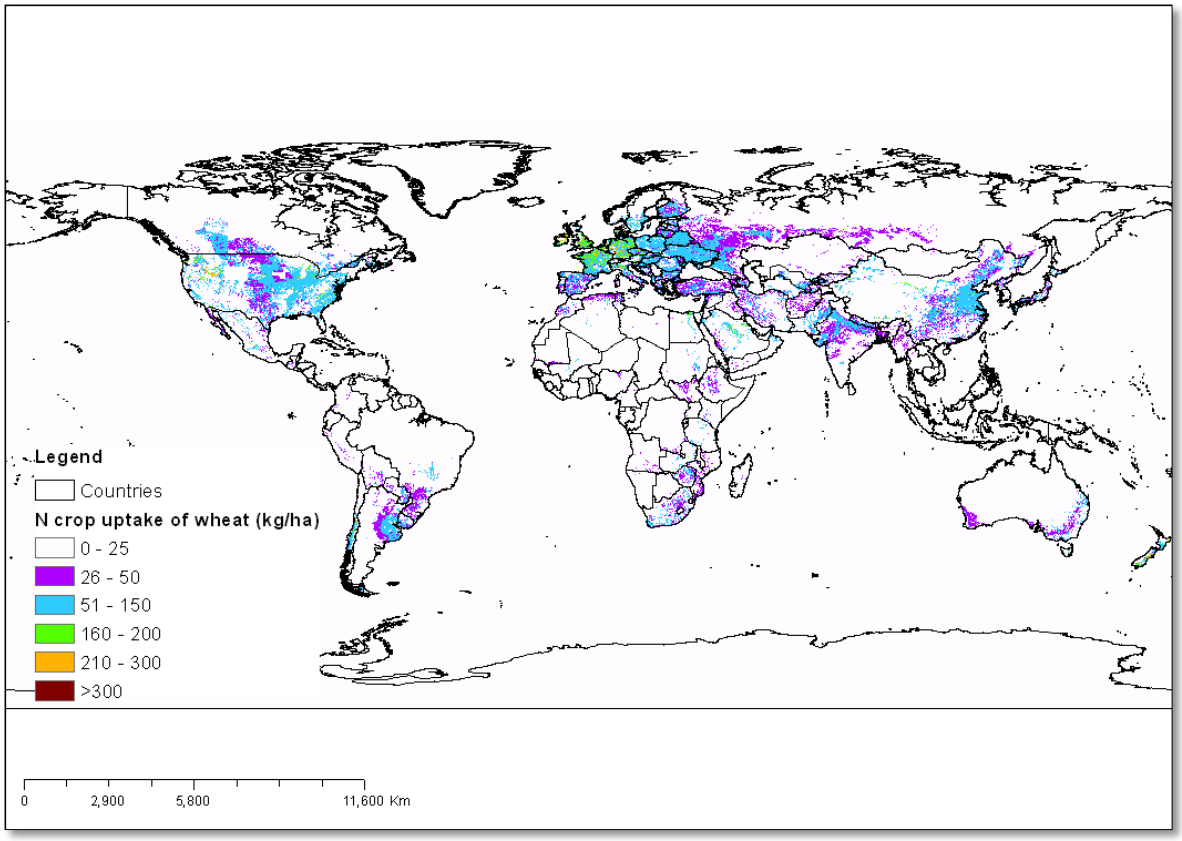

Figure 4. Global spatial distribution of crop nitrogen uptake for wheat (kg/ha)

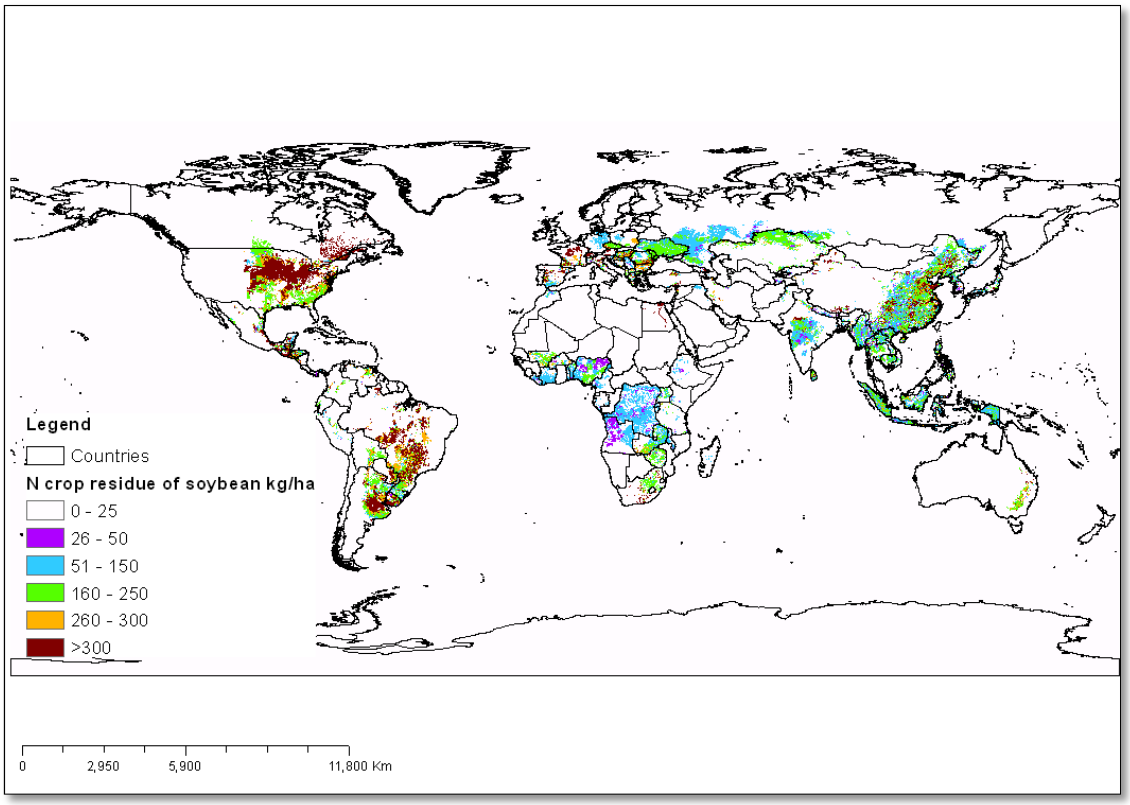

Figure 5. Global spatial distribution of nitrogen residue of soybean (kg/ha)

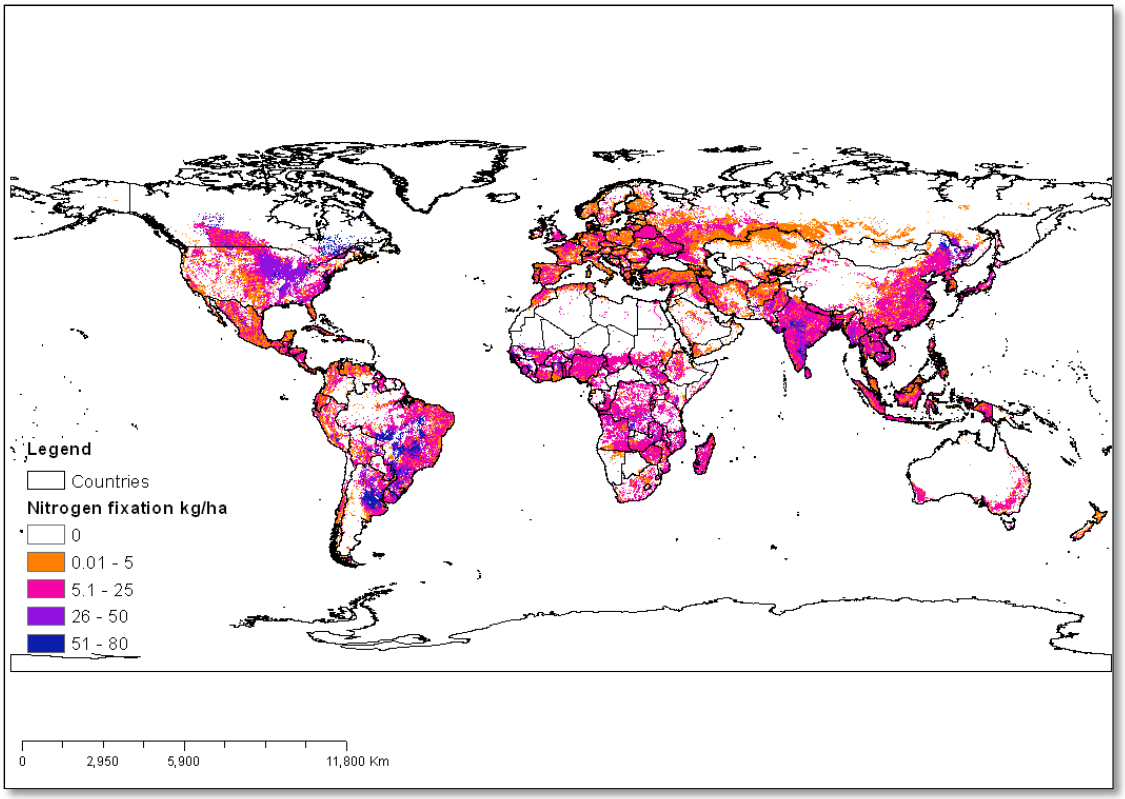

Figure 6. Global spatial distribution of total nitrogen fixation (kg/ha)

3.3 Mineral and manure fertilizers

Mineral fertilizers data were gathered from FAOSTAT, International Fertilizers Association (IFA) and other international sources (EUROSTAT, USDA, WTO, World Bank, etc.). The data consisted in total used fertilizer per country including total nitrogen (TN), total phosphorus (TP) (available as P2O5 and converted in total elemental phosphorus) and urea consumption obtained from IFA. A percentage of total TN and TP fertilizers in each country was applied to grass land according to the percentages reported in Lassaletta et al. (2014) for the year 2005. In some particular cases these coefficients were adjusted based on literature information, and for New Zealand, Bahrain and Oman the percentage of mineral of fertilizers applied to grassland was set to 70%, 50%, and 50%, respectively.

To take into account gaseous losses of applied fertilisers we used an emission factor approach. For the calculation of NH3 losses into the atmosphere we adopted the emission factor (% NH3 losses of N content) reported in Bouwman et al. (1997) by fertilizer categories and by zone (temperate and tropical zones as the temperature impacts the volatilization of NH3). Consequently, we classified each country as belonging either to the temperate or tropical zones based on its latitude.

Since urea is the most commonly used mineral fertilizers in the world (Riddick et al, 2016), accounting for more than 50% of global N mineral usage, we split the total nitrogen applied in two fertilizer categories: urea and others. For the percentage of mineral fertilizers that is urea we applied gaseous emission loss factors of 15% and 25% in temperate and tropical zones, respectively. For the other nitrogen fertiliser types we applied a factor of 3.5% as the mean of emission factors of all fertilizers categories reported in Bouwman et al. (1997) excluding urea. The emission rate of N20 was retrieved from FAOSTAT and amount of 1%, similar to that reported in Bowman et al. (2002) of 0.9%. NO emission rate was set to 0.7% as reported in Bowman et al. (2002).

The net amount of applied mineral fertilizers (total amount minus gaseous losses) was then distributed at grid level in each country based on the distribution of crop uptake, while on grassland the net mineral fertilizer was distributed based on the grass area inside each grid cell. A part of the net TN mineral fertilizer was applied on fodder grazing (FODG class) only when the nitrogen uptake of the fodder grazing was lower than the sum of the applied nitrogen manure fertilizer and nitrogen fixation. Figure 7 and Figure 8 show the global raster map of TN and TP fertilizer application.

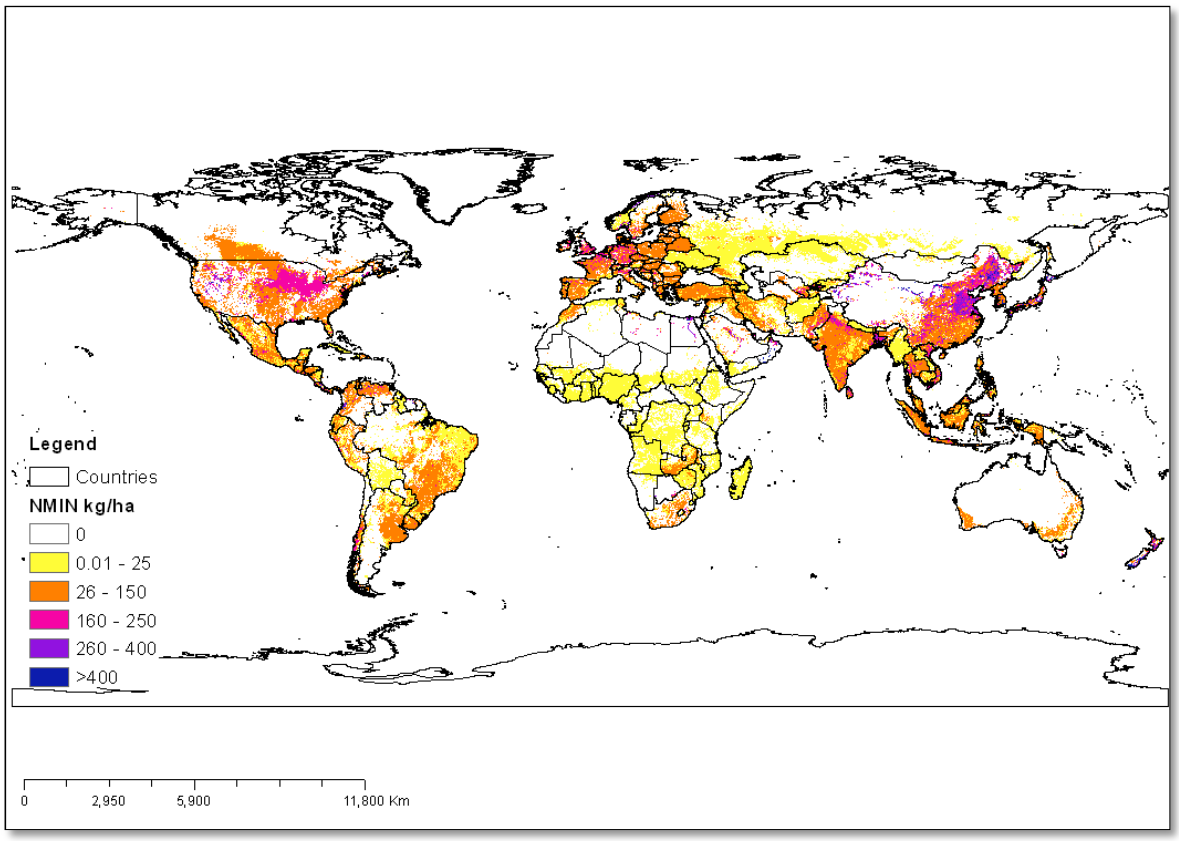

Figure 7. Global spatial distribution of TN mineral fertilizers applied (kg/ha)

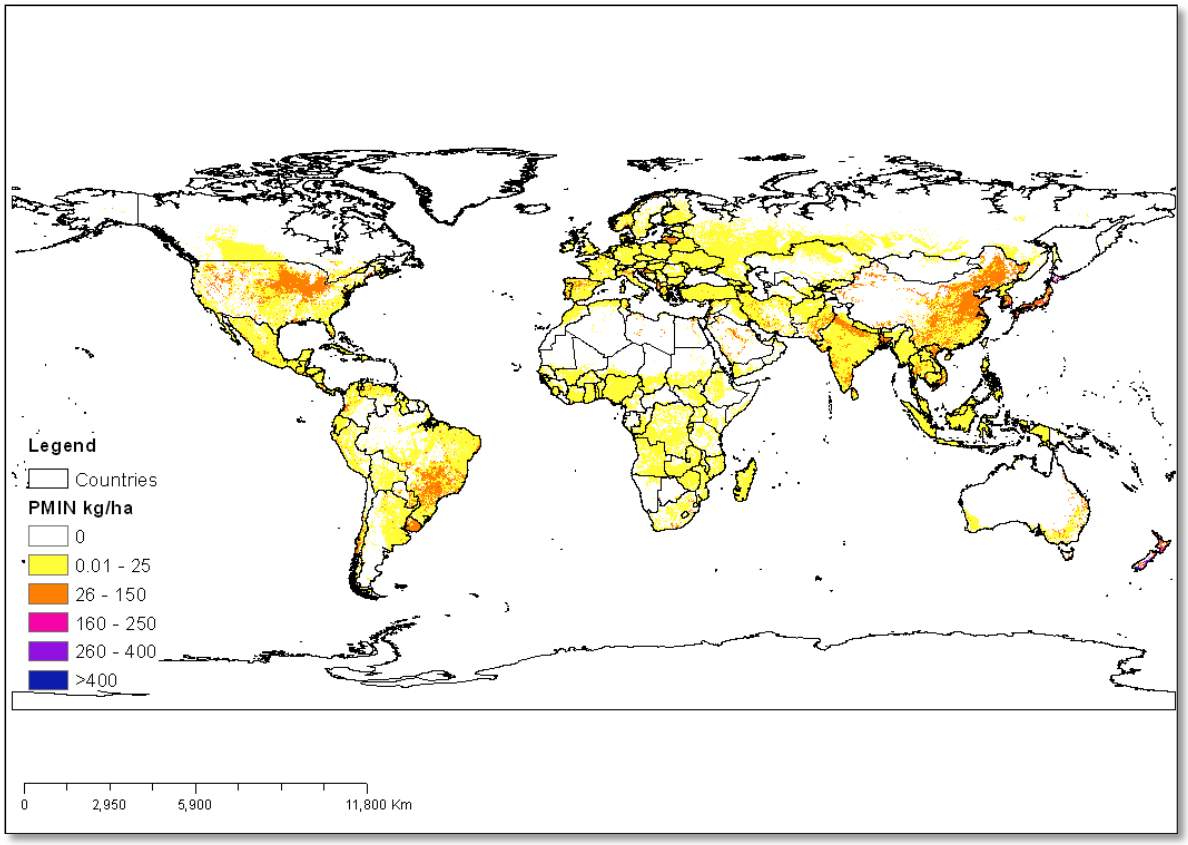

Figure 8. Global spatial distribution of TP mineral fertilizers (kg/ha)

The amount of nitrogen and phosphorous originating from manure was computed for each cell multiplying the number of animal category (in heads) by the excretion coefficients per animal category (kg N or P/head year).

The excretion coefficient for the year 2005 used in this study were calculated using the N excretion coefficient given in Bowman et al (1997) and the slaughtered weights (Yield/Carcass) from FAOSTAT following the procedure reported in Sheldrick et al (2003).

Livestock numbers for six animal categories were extracted from six raster maps retrieved from GeoNetwork rasters (Geonetwork FAO spatial data) at 0.05 decimal degrees resolution. These rasters were resampled to a coarser resolution of 0.083 decimal degrees (5-minutes) as base rasters for distributing 16 FAOSTAT categories of livestock in each country for year 2005. Cattle, chickens, ducks, goats, pigs, sheep were spatially distributed based on the corresponding spatial distribution from GeoNetwork. The sum of Camelidis and Camels was distributed on BARE landcover class proportional to its area in each pixel. A similar approach was used to distribute Buffaloes on GRAS land cover. Mules, horses and asses were distributed using the spatial distribution of Cattle from GeoNetwork. Geese, pigeons and turkeys were spatially distributed based on the sum of chickens and ducks, while animal live nes and rabbits were spatially disaggregated using the total livestock distribution.

The calculation of manure fertilizers at grid cell scale followed the procedure described in Bouwman et al (1997). Concerning the nitrogen, for each category of livestock, the number of animals in each grid cell was multiplied by N excretion coefficients that differed between developed and undeveloped country and stable and meadow type of production. Allocations of manure between stable and meadow are more relevant for developed countries, particularly for Europe and North America (Liu et al., 2010). Thus,

in developed countries, manure produced in stables was considered to be around 90% of total manure while in undeveloped countries it was set to 66%. These percentages were adopted for each category of livestock excluding pigs and poultry for which the percentage of manure on stable was set to 90% in all countries. We considered for each country that the stable manure was applied only on arable land, while the meadow type of manure was applied on FODG, GRAS, BARE and SHRU landcover classes proportionally to their areas.

The gaseous losses during excretion were estimated using specific volatilization rates of different livestock category reported in Bouwman et al, (1997). N2O emission were calculated from the FAOSTAT by country and livestock category, while for NO emission we adopted a percentage of 0.7 as reported in Bowman et al. (2002).

A similar procedure was applied to quantify the phosphorus manure considering that its excretion factor is a percentage of nitrogen excretion factor.

The distribution of manure produced in stables and meadows for each category of livestock in each grid cell was calculated as follows: the manure produced in stable for each grid was distributed on arable land of the grid cell (ARAB class) with a maximum limit of 50 kg/ha. The remaining part was distributed together with meadow type manure on FODG again with a limit of 50 kg/ha and the remaining part on GRAS, BARE and SHRU land cover class inside the same grid cell. The manure produced in meadow for each livestock class was distributed proportionally to the area between FODG, GRAS, BARE and SHRU category in each grid cell. It was assumed that the manure fertilizer was only applied in non-nitrogen fixing crops and it was distributed based on the crop uptake. Figure 9 and Figure 10 show maps of total TN and TP manure fertilizer application.

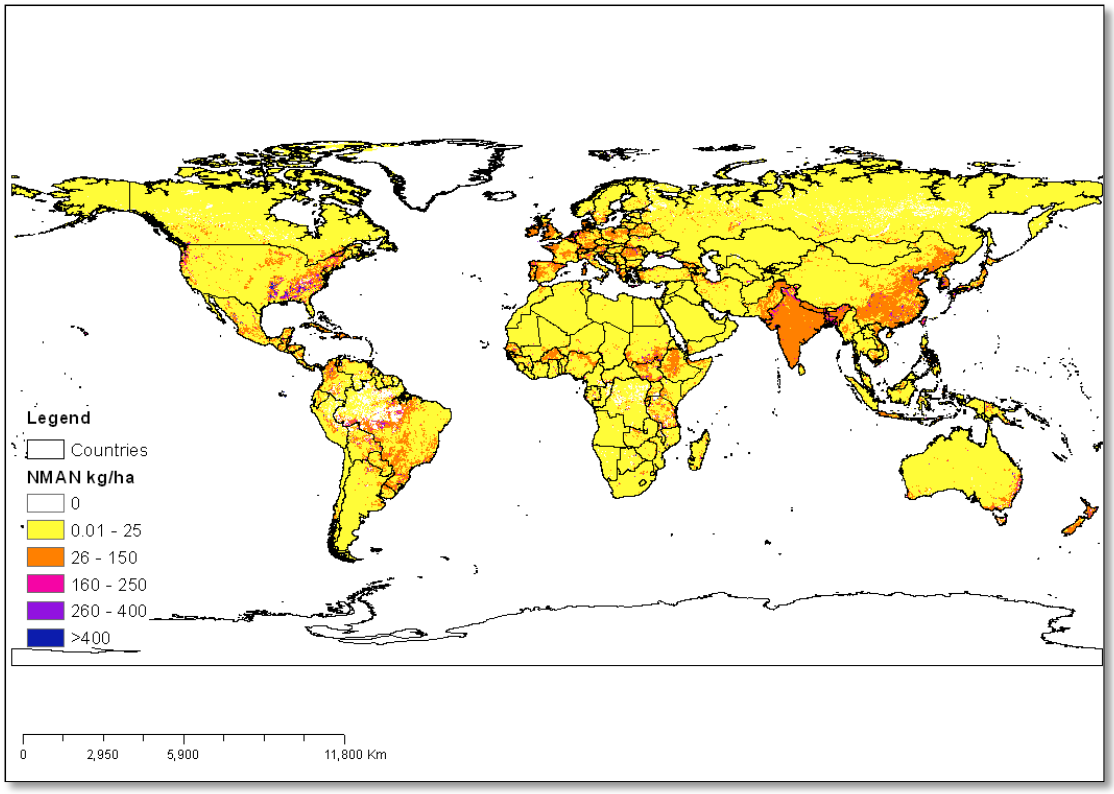

Figure 9. Global spatial distribution of TN manure fertilizers (kg/ha).

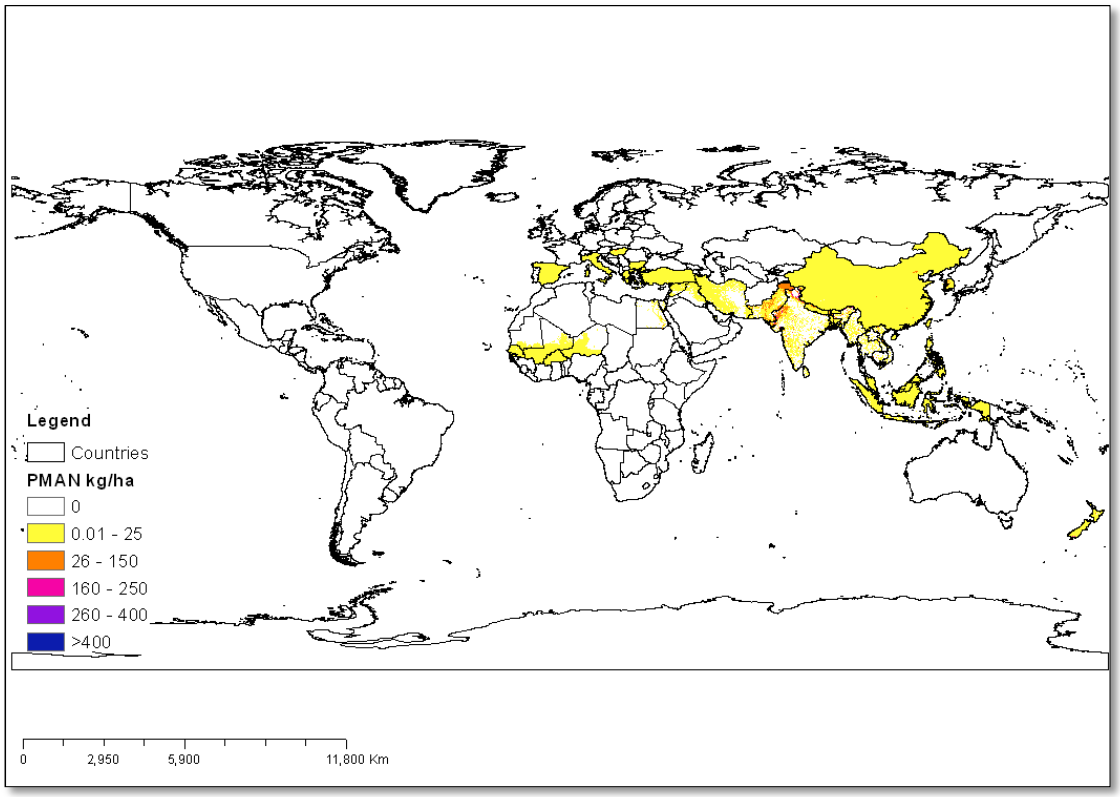

Figure 10. Global spatial distribution of TP manure fertilizers (kg/ha)

3.4 Human waste and industrial discharge

3.4.1 Domestic nutrient emission

Point source emissions are estimated according to the methodology described by Grizzetti and Bouraoui (2011). The procedure includes the collection of national statistics of household connection to sewers, connection to wastewater treatment plants and then the degree of treatment. The second step is then to estimate the per capita nitrogen and phosphorus emissions. Then a downscaling approach based on population density, urban and rural population is used to estimate at the grids level the pollutant load from domestic use of water. The N and P emission from human excretion was derived from a procedure developed by Jönsson & Vinnerås (2004), in which the N and P emissions are related to the human protein intake taken from the FAO database (FAOSTAT, 2016) as follows:

Equation 4 $$N_{emission} = 0.11 * TFProtIntake$$

and

Equation 5 $$P_{emission} = 0.010 * (TFProtIntake + VegProtIntake)$$

where $N_{emission}$ is the human emission of nitrogen (g N/yr/person), $P_{emission}$ is the human emission of phosphorus (g P/yr/person), TFProtIntake is the total food protein intake (g/yr/person) and VegProtIntake is the vegetable protein intake (g/yr/person). The data for total and vegetable protein intake was retrieved from the FAO (FAOSTAT, 2016). The data retrieved from the FAO was then adjusted to consider food waste and losses using correction factors derived from FAO (2011) and given in Table 2:

Table 2. Percentage of food waste according to different geographical regions (FAO, 2011)

	Europe inc. Russia	N.Ameri. & Oceania	Industri. Asia	Sub.-S Africa	N. Afri. & W. C. Asia	S. & S. east Asia	Latin America
Cereals	25	27	20	1	12	3	10
Roots & tubers	17	30	10	2	6	3	4
Oilseeds & pulses	4	4	4	1	2	1	2
Fruits & vegetables	19	28	15	5	12	7	10
Meat	11	11	8	2	8	4	6
Fish & seafood	11	33	8	2	4	2	4
Milk	7	15	5	0.1	2	1	4

The overall formula to calculate the net nutrient emission is thus as follows:

Equation 6 $$NE_{N,P} = POP\left(E_{N,P}\left[1 - WAS\right]\right)$$

where $NE_{N,P}$ is the net emission of nutrient (nitrogen,[N]; phosphorus [P]), POP is the population, $E_{N,P}$ is the per capita emission of nutrient calculated independently at national scale for nitrogen and phosphorus, and WAS is the percentage of food waste according to Table 2.

Then it is assumed that 3% of the nitrogen and phosphorus intake is lost via seat, hair and blood (Calloway and Margen, 1971; Morée et al., 2013). No pattern could be found to distinguish between eating habits of urban and rural population, and consequently the net emission was assumed to be the same in urban and rural areas

The flow chart to estimate point sources and scattered dwellings is illustrated in Figure 11.

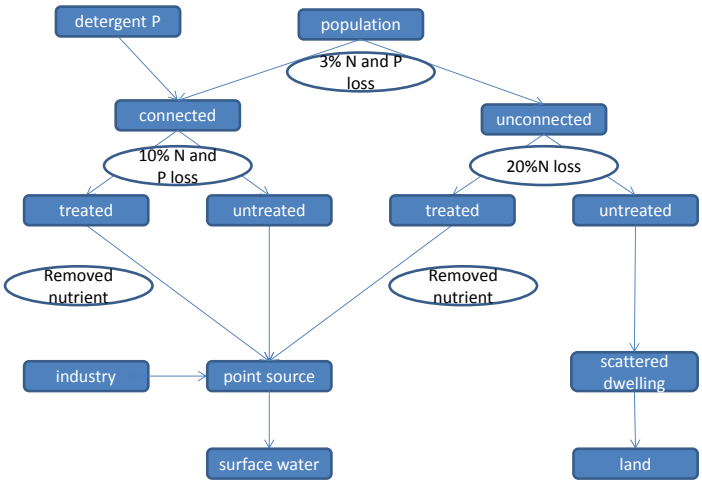

Figure 11. Flow chart for the calculation of points sources and scattered dwellings.

It can be seen that the net emission from the population can follow two main pathways: connected to sewers where a treatment could be applied or unconnected and in such case there could be no nutrient removal and consequently the total load is discharged untreated as point source in surface water. The connection rate and treatment level for Europe (EUROSTAT data) and OECD countries are listed in Table 2 (latest year available). It is assumed (Morée et al., 2013) that leakages, biological degradation, particulate nutrient settlement and volatilization account for about 10% of the net nutrient emissions entering the sewer system. For unconnected people it is assumed that the 10% of the net emission of nitrogen is lost via volatilization (Morée et al., 2013).

When the sum of the connection rate of primary, secondary, and tertiary treatment is lower than the connection rate to sewer, then the difference is assumed to be discharged untreated in surface water. When the sum is larger than the connection rate to sewer, then a part of the wastewater from unconnected people is then also treated. This is the case of countries where trucks go around collecting wastewater from individual households and taking the waste to treatment plants. For the unconnected fraction of population, a more detailed description of the sanitation type was retrieved from the JUMP Surveys (WHO, 2016). In particular we retrieved information on the fraction of improved and unimproved sanitation for both urban and rural population. We also retrieved the specific types of sanitation including septic tanks, latrines (improved and unimproved), and open defecation that poses a serious health problem in some developing countries).

Table 3. Connection and treatment level for Europe and OECD countries

country	1 ary treatment (% population)	2 ary treatment (% population)	3 ary treatment (% population)	connection sewer (%)
Albania	18	18	18	78.1
Austria	0	1	93.5	94.5
Belgium		11	73	88.5
Bosnia Her	0.1	1.2	0.6	35.2
Bulgaria	1.9	19.3	35.3	74.7
Croatia	11.7	26.3	0.6	53
Cyprus	0	11.5	18.3	29.8
Czech Republic	0.2	8.2	71.6	84.7
Denmark	0	2	88.2	91
Estonia	0	5	78	82
Finland	0	0	83	83
France	0.2	15.2	66.1	81.5
Germany	0	3	93	97.3
Greece	0	6.3	85.8	92
Hungary	0.1	16.1	56.5	75
Iceland	57	0	1	91
Ireland		47	18	69
Italy	11.4	4	78.6	94
Latvia	3.7	50	17.2	71.1
Lithuania	0	2.4	60.7	74.1
Luxembourg	2	27	70	100
Malta	7.1	92.9	0	100
Netherlands	0	0.3	99.1	99.4
Norway	19.3	1.4	61.2	85.3
Poland	0	14	58	72
Portugal	3.6	39.4	16.4	81.3
Romania	7.4	19.2	18.3	47.1
Serbia	1.2	7.8	1.6	57.8
Slovak Republic		27.8	27.2	64.7
Slovenia	0.5	33.2	21.7	62.6
Spain	0.6	28.1	66.7	99.1
Sweden	0	4	83	87
Turkey	16.3	20.2	21.8	83.8
United Kingdom	0	43	57	97.3
Australia[1]	25	55	14.5	94.5
Canada	16	53	15	87
Chile	24	4	63	96
Israel	6	40	50	98
Japan	1	55	20	76
South Korea	0	36	54	90
Mexico[2]	10.3	42.1	0.2	71
New Zealand[3]	0.8	1.2	80	82
U. S. of America	2	32	40	74

[1] Adjusted using data from "Human Settlements by CSIRO"; [2] data adjusted using data from Mexican Ministry; [3] data using OECD latest and older data

N and P removal for primary, secondary, and tertiary were taken from Morée et al. (2013), while BOD and faecal coliform are from Fuhrmesiter et al. (2015) and World Bank (2008) The efficiency of the different systems are summarized tin Table 4.

Table 4. Nutrient and BOD removal efficiency for the various sanitation and treatment types

	Nitrogen removal (%)	Phosphorus removal (%)	BOD removal (%)	Faecal coliform removal (%)
primary	10	10	30	90
secondary	35	45	85	99
tertiary	80	90	85	99
septic tank	30	35	35	90
pit latrine	30	35	35	90

3.4.2 Industrial emissions

As no global database on the national emission of nitrogen and phosphorus was available, the nitrogen and phosphorus industrial emission were estimated as 15% of the human emission as suggested by Morée et al. (2013).

3.4.3 Phosphorus emissions from detergents

Data on the world wide use of sodium triphosphate (STP) in detergents is very limited. Several countries have limitations or bans on the use of P-based detergents. To estimate the use of P-based detergents throughout the world we selected few countries that have no ban or limitation on the use of STP in detergents including Cyprus, Czech Republic, Estonia, Greece, Hungary, Latvia, Lithuania, Malta, Poland, Portugal, Slovak Republic, Spain, United Kingdom, Bulgaria, Romania, Moldova, Ukraine, Albania, Bosnia Herzegovina, Croatia, Serbia, Macedonia FYR, China, India. The data from European countries were retrieved from Bouraoui et al. (2012). The data from India was retrieved from Kundu et al. (2015), while for China the data was taken from Chen et al. (2015). The STP –detergents consumed was then plotted against the GDP for year 2005 and the results are shown in Figure 12.

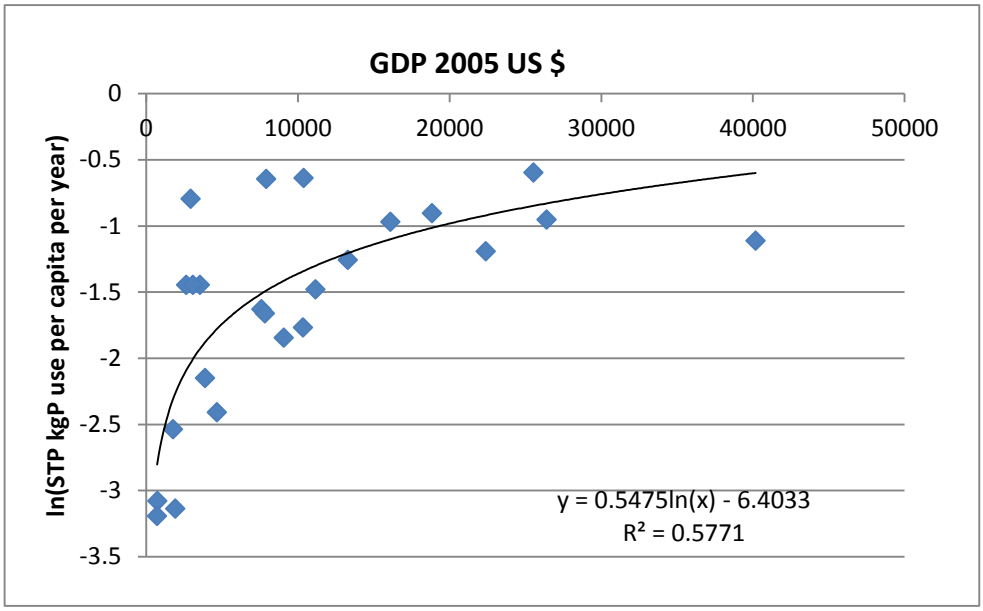

Figure 12. STP-detergent versus GDP per capita in 2005.

When data was not available for a specific country, the consumption was estimated based on the regression equation given in Figure 12, while if data was available it was used as is.

To evaluate the coherence of the data and of the assumptions made, we calculated the emissions of nitrogen and phosphorus at global scale. The results for year 2005 are summarized in Table 5.

Table 5. Summary of Global emission source for nitrogen and phosphorus

	N EMISSIONS TG YR^{-1}	***P EMISSIONS TG YR^{-1}***
DOMESTIC	16.34	2.44
DETERGENTS		0.90

The phosphorus from human excreta amounted to 2.94 Tg which is completely online with the estimates of Chen and Graedel (2016) and Liu et al. (2008). It was just

estimated that approximately that 0.5 Tg of phosphorus was removed in urban wastewater treatment plants. The total estimate of P from detergents (STP) amount to 0.90 Tg that is compatible with the estimate of STP production that amounts to 0.86 in 2004 (Liu et al., 2008).

3.5 The global spatial distribution of point sources and scattered dwelling

The point sources and scattered dwellings calculated at country level were distributed in each grid cell based on the rural and urban population count inside each grid cell given by the GHSL datasets (Dijkstra and Poelmann, 2014) at resolution of 1 km. The rural and urban population distribution of the GHSL dataset refer to year 2015 and thus were rescaled to 2005 using the FAOSTAT values that provide for each country the rural and urban population counts.

The basic assumption to assign the connection rate was that the more densely populated areas are more likely to be connected to a central sewage system when present. The rescaling procedure for connected urban and rural population consisted in the selection of the grid cell with the highest population ordered by groups of 9 grid cells until the target value of connection was reached. Figure 13 and 14 show the global spatial distribution of urban and rural population connected to a central wastewater treatment plant.

The population non-connected was then non-assigned population from the previous step. Figures 15, 16, 17 and 18 show the distribution of N emissions at global scale from urban and rural connected population while Figure 19 and Figure 20 show the spatial distribution of N emissions from unconnected population ("improved" category).

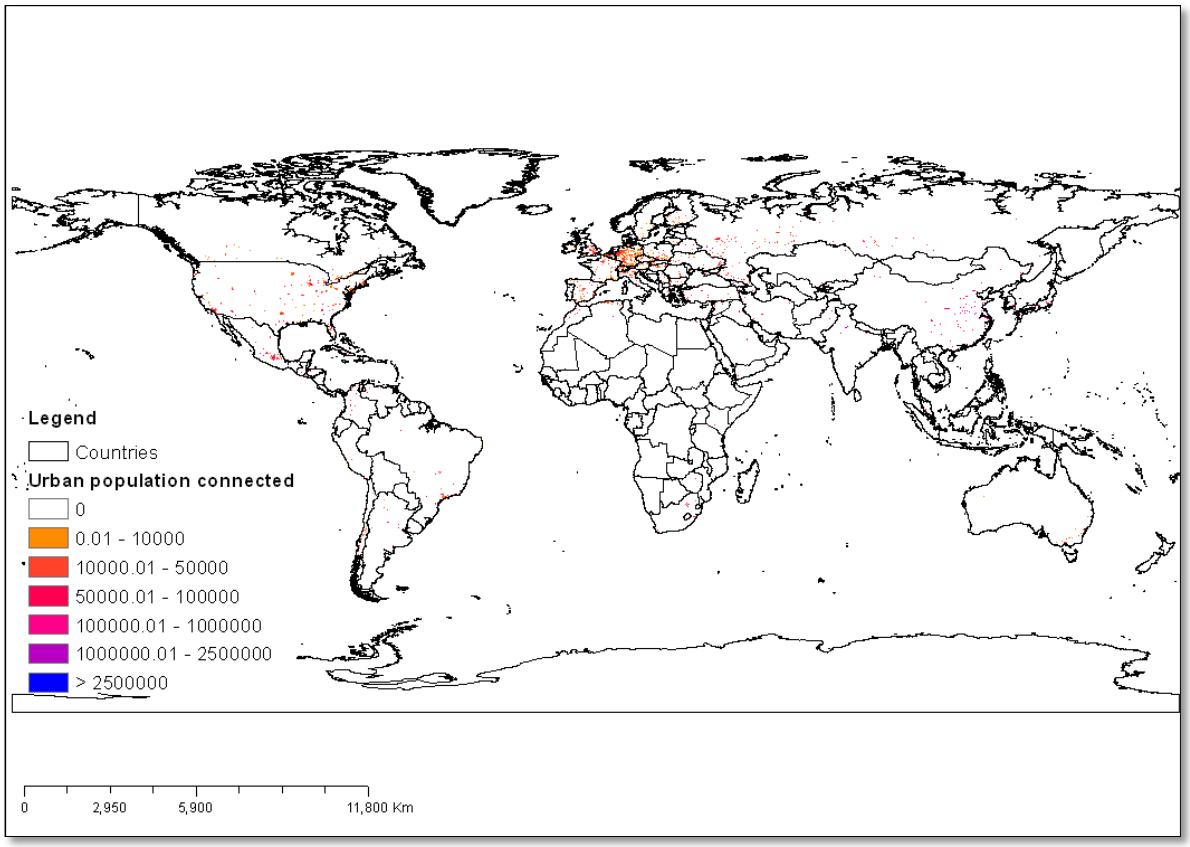

Figure 13. Global spatial distribution of urban connected population

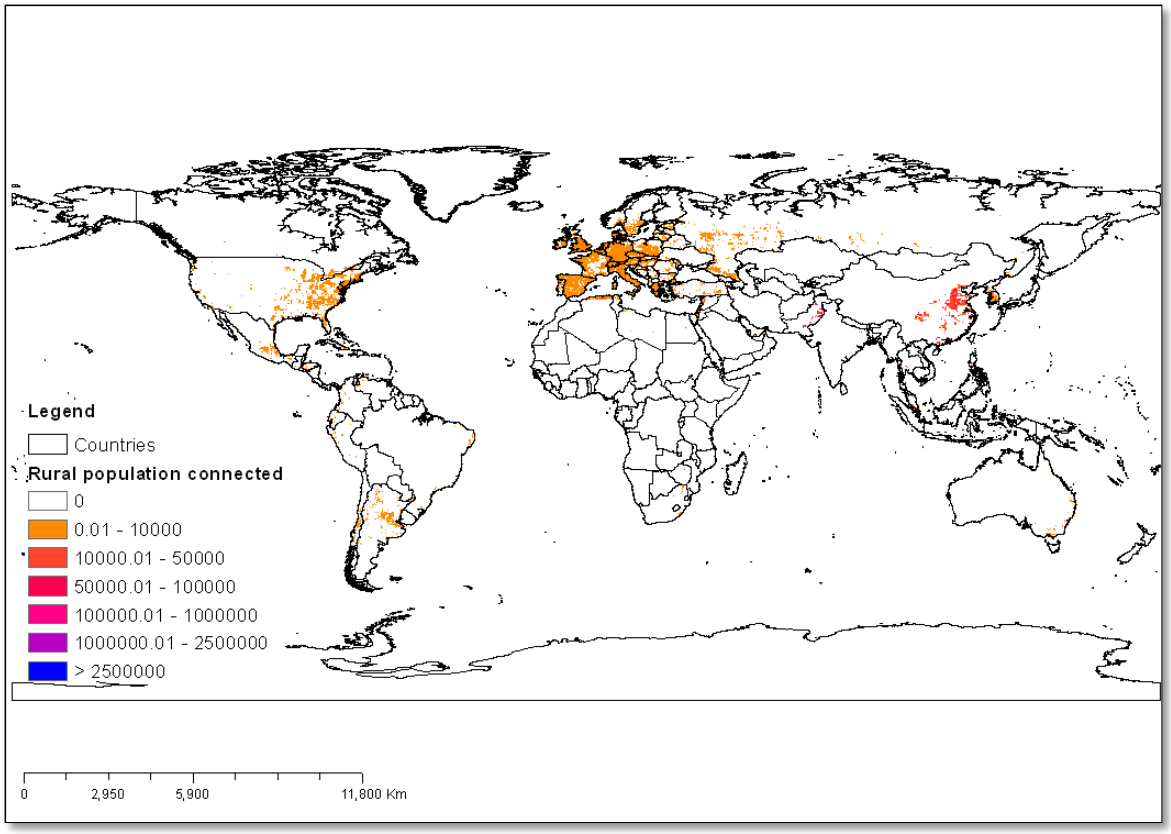

Figure 14. Global spatial distribution of rural connected population

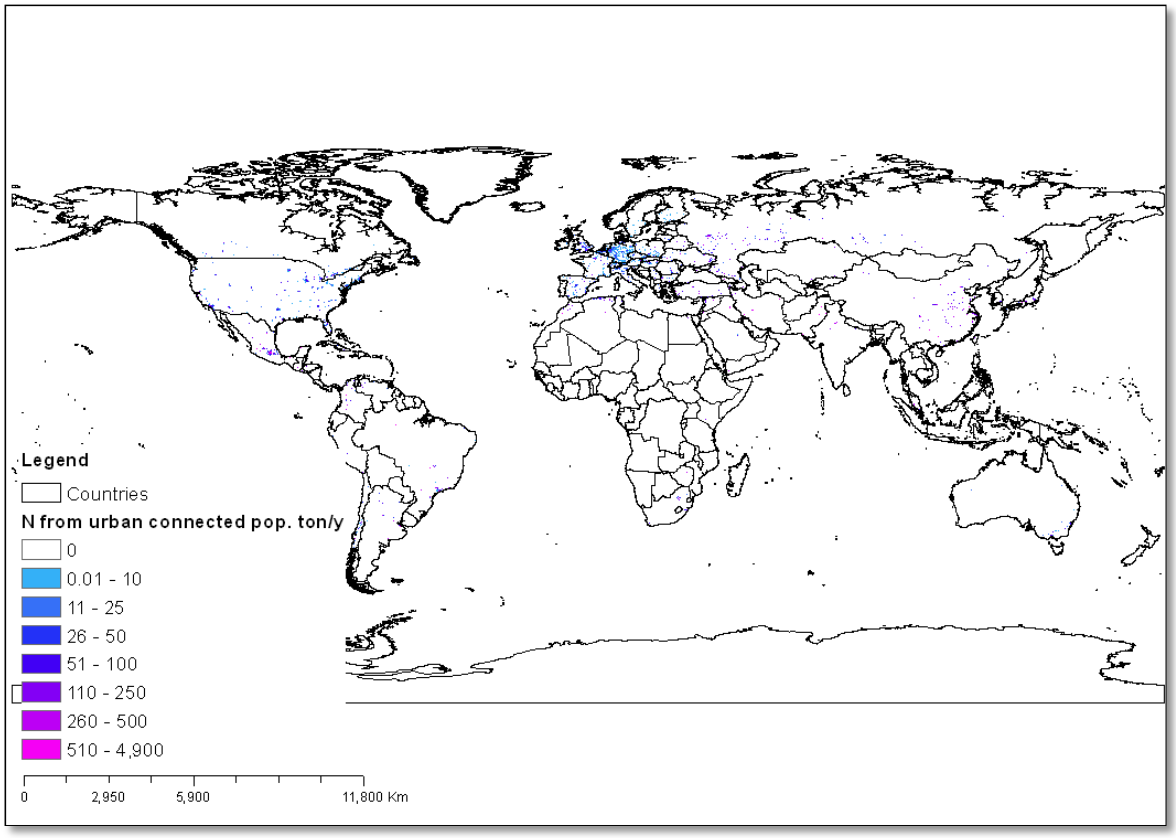

Figure 15. Global spatial distribution of N emission (ton/y) from urban connected population

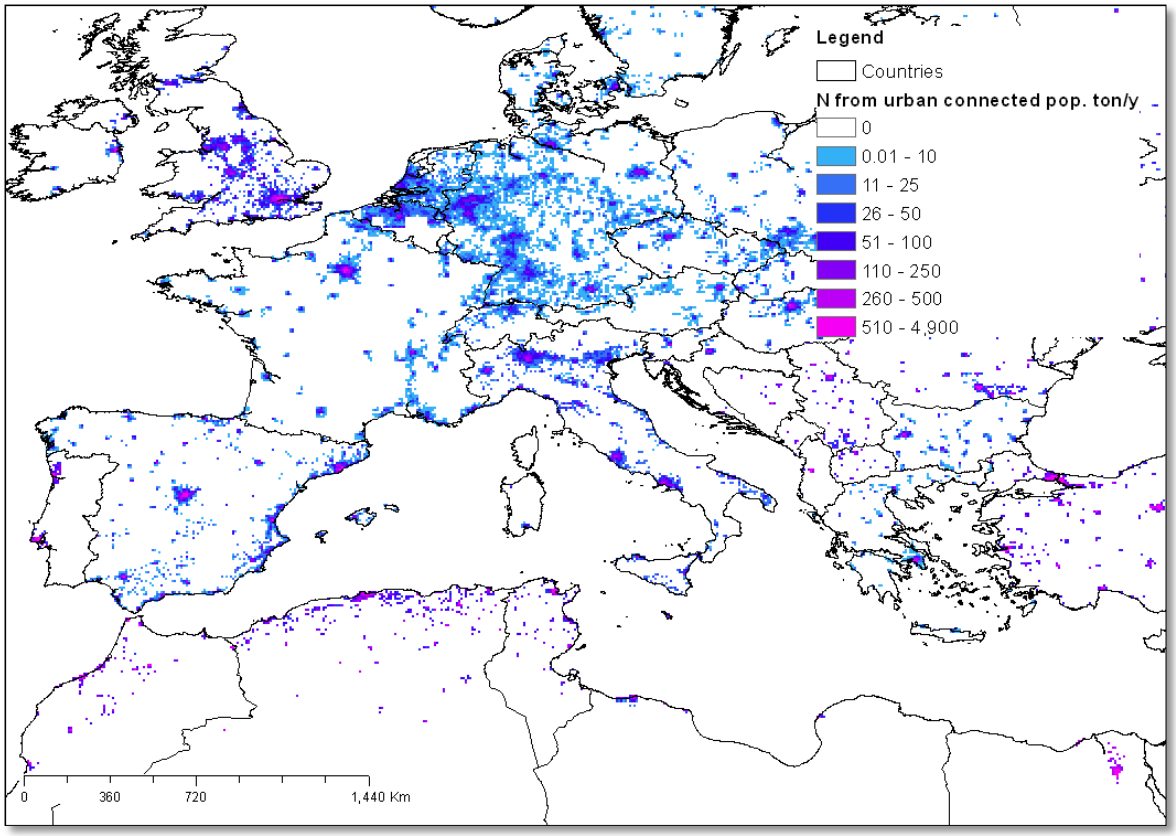

Figure 16. Spatial distribution of N emission (ton/y) from urban connected population (focus Mediterranean area)

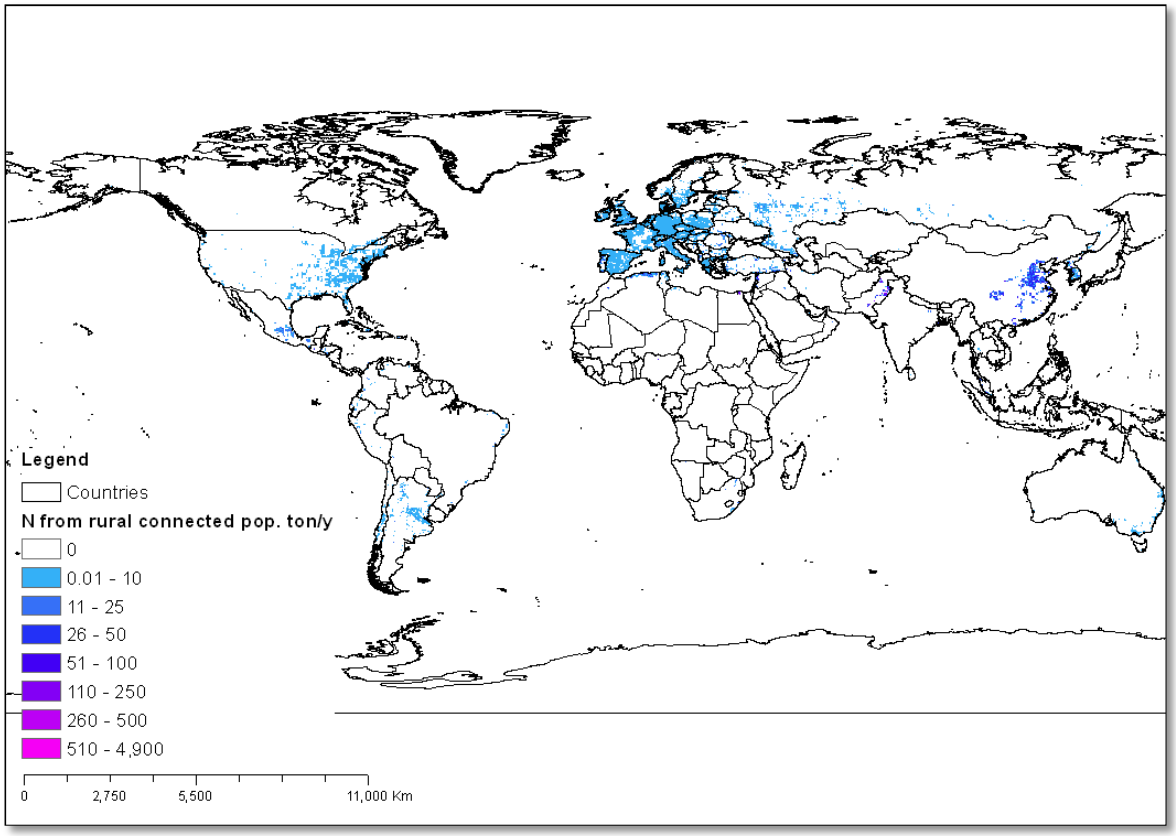

Figure 17. Global spatial distribution of N emission (ton/y) from rural connected population

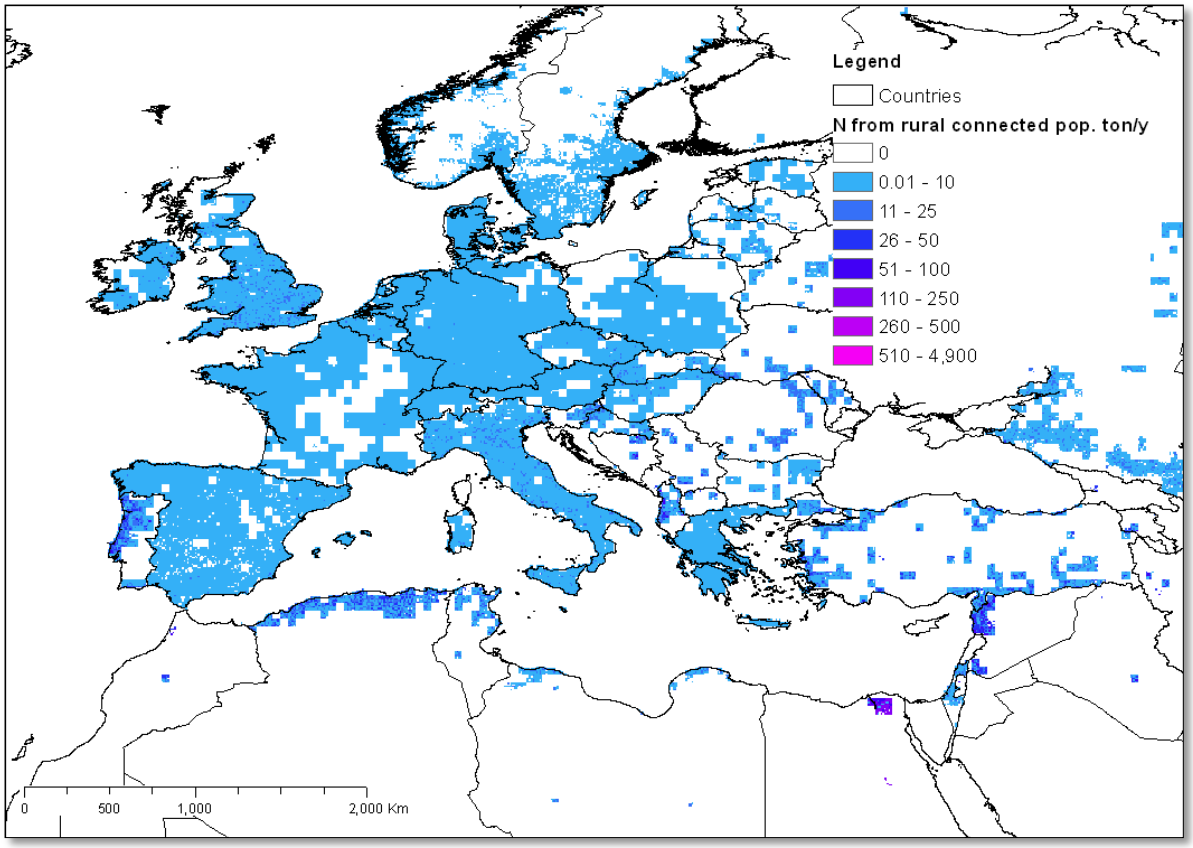

Figure 18. Spatial distribution of N emission (ton/y) from rural connected population (focus Mediterranean area)

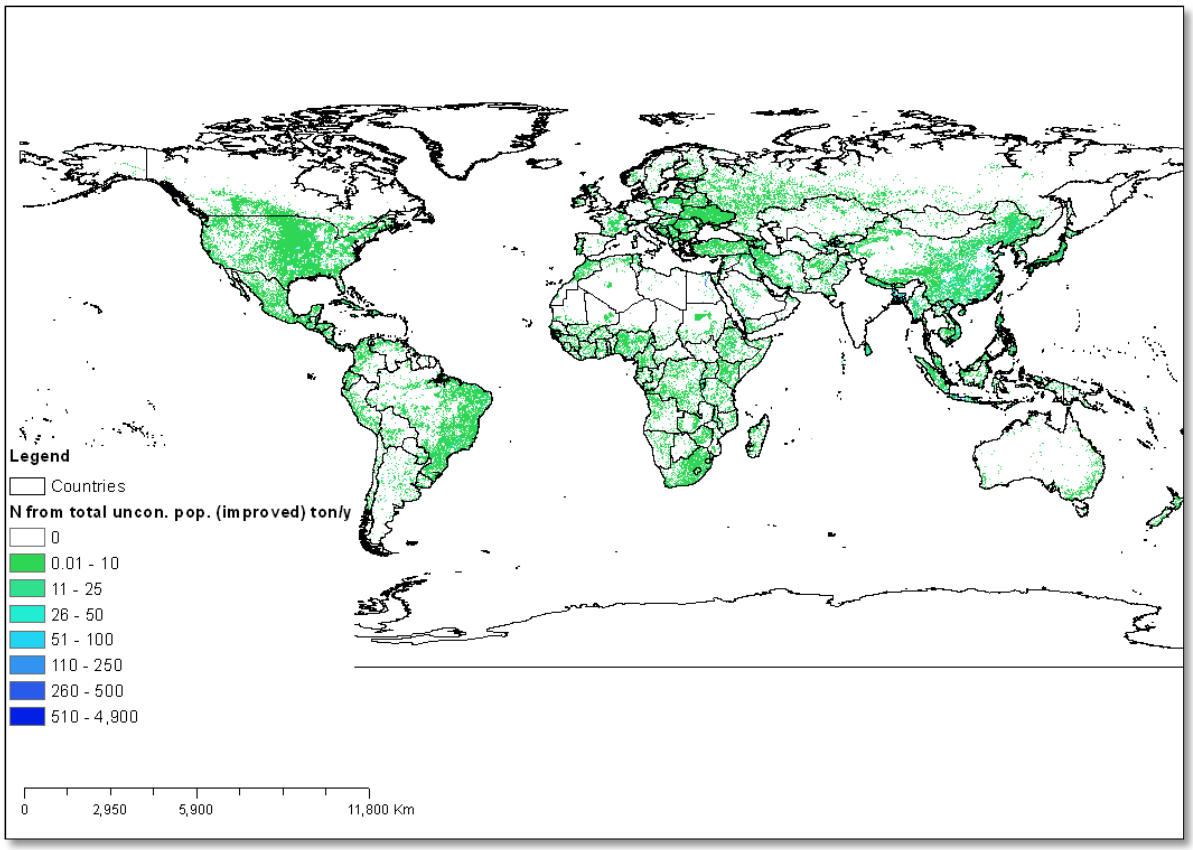

Figure 19. Global spatial distribution of N emission (ton/y) from total unconnected population ("improved" category)

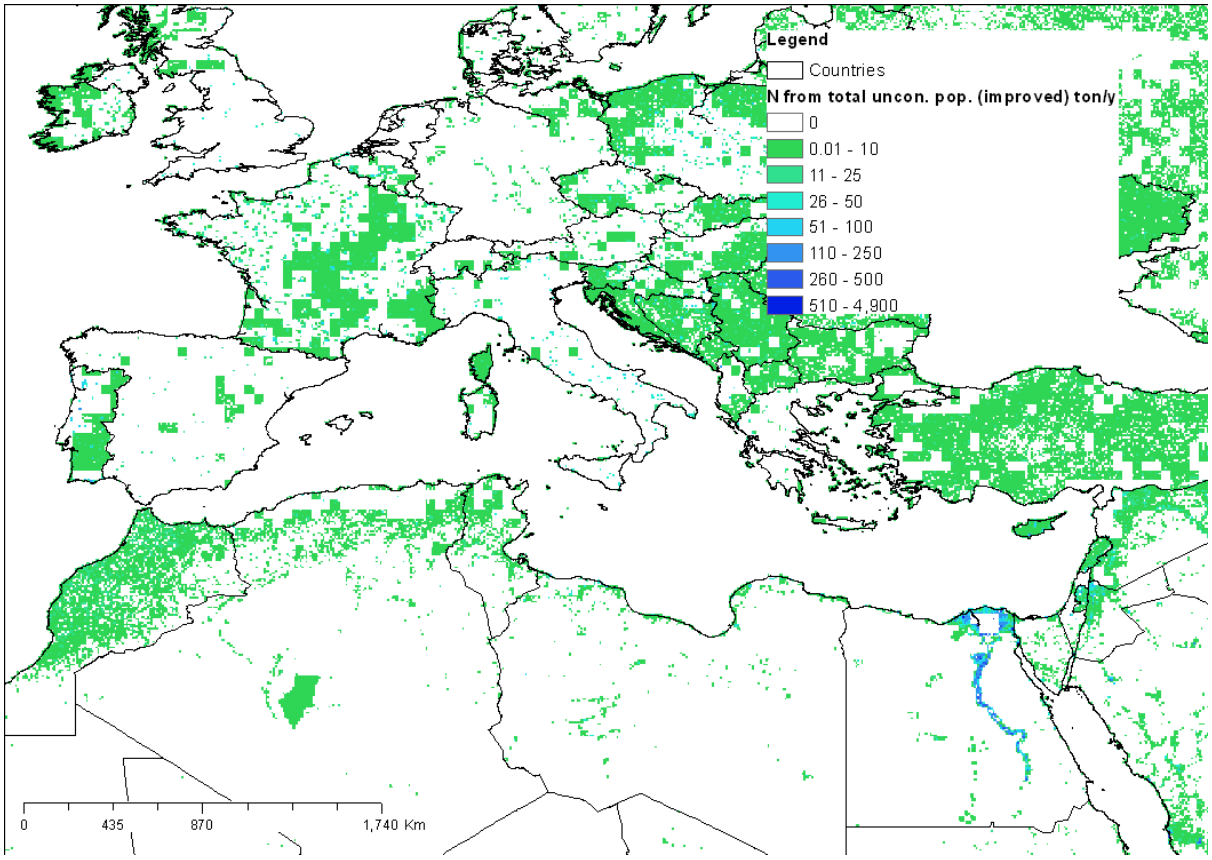

Figure 20. Spatial distribution of N emission (ton/y) from total unconnected population ("improved" category) (focus Mediterranean area)

3.6 Atmospheric deposition

Atmospheric deposition of nitrogen plays a key role in the overall nitrogen balance. Vet et al. (2014) undertook a large effort under the direction of the World Meteorological Organization (WMO) Global Atmosphere Watch (GAW) Scientific Advisory Group for Precipitation Chemistry (SAG-PC) to produce a high quality global data of precipitation composition and deposition of major ions. This resulted in quality assured global data set of wet deposition monitoring data for 2000–2002 and 2005–2007. This dataset was used in an ensemble modelling effort including 21 global chemical transport models resulting in gridded global and regional maps of major ion concentrations in precipitation and deposition (Vet et al., 2014). The data was retrieved from the World Data Centre for Precipitation Chemistry web site (http://wdcpc.org/).

The data is available on a 1 degree resolution and consist of rasters of wet and dry deposition (kgN/ha) of oxidized and reduced nitrogen. In particular, we used the raster combining all forms of nitrogen deposition (FWD_TON) for the period 2005-2007. Figure 21 shows the spatial distribution of total nitrogen deposition in kg/ha at global scale. The distribution of total nitrogen deposition between the landcover classes in each grid cell was proportional to the area of each class.

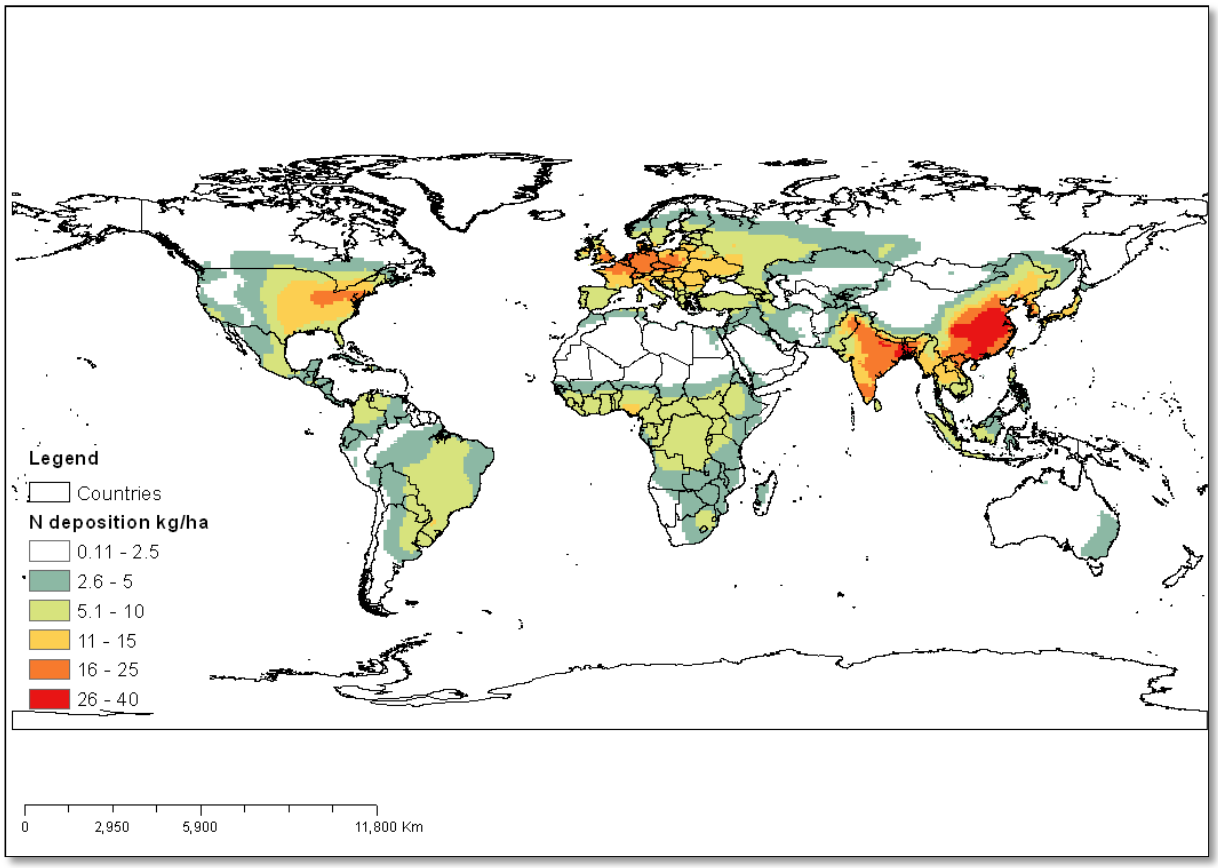

Figure 21. Global spatial distribution of nitrogen deposition (kg/ha)

3.7 Hydrography and routing

The river network and routing structure was retrieved from HydroSHEDS (Hydrological data and maps based on SHuttle Elevation Derivatives at multiple Scales; Lehner et al., 2008). HydroSHEDS is based NASA's Shuttle Radar Topography Mission (SRTM). The HydroSHEDS provides information at various spatial resolution (3, 15 and 30 arc-seconds) layers of void-filled DEM, flow direction, flow accumulation, river network and drainage river basins.

We developed a procedure to extract a low resolution (5-minutes) river networks from high resolution digital elevation such as the HydroSHEDS routing at 30 arc-second. We followed a procedure proposed by Olivera et al. (2002) using only the flow accumulation and the low resolution grid cells. Figure 22 shows the comparison between the drainage area of the basins created from the river networks at 5- minutes of resolution with those of HydroSHEDS. An extract of the derived river network is shown in Figure 23.

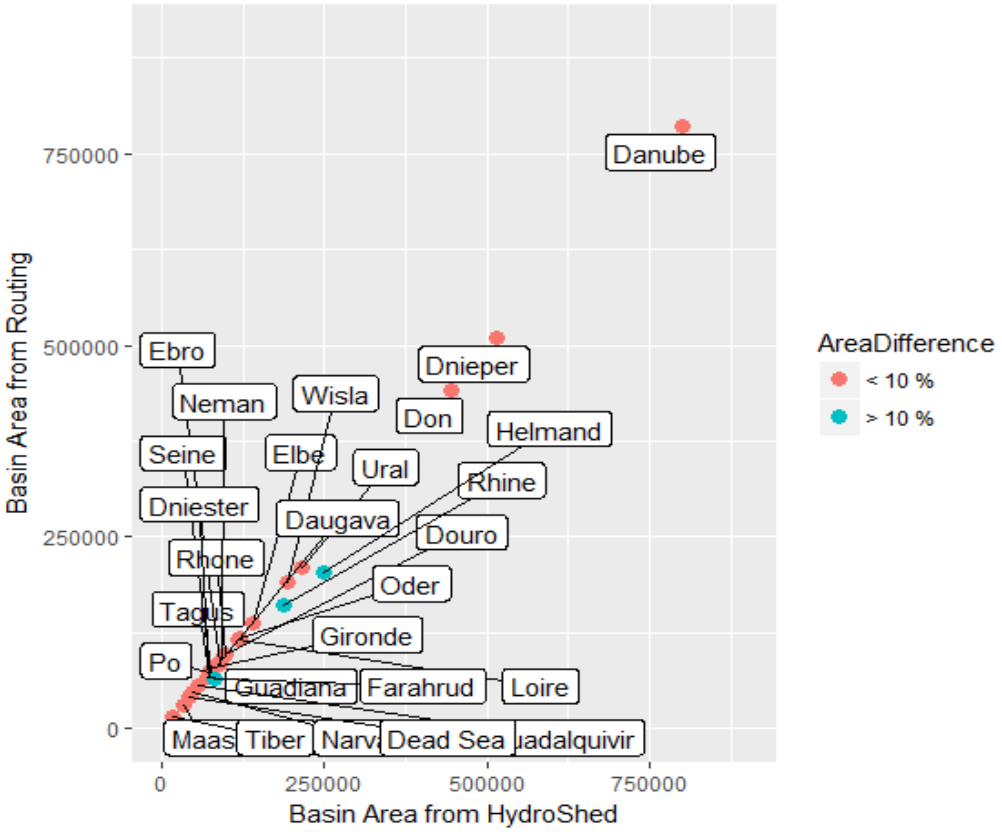

Figure 22. Comparison between the drainage area of basins in Europe obtained from the new river network at 5-minutes and HydroSHEDS Basins.

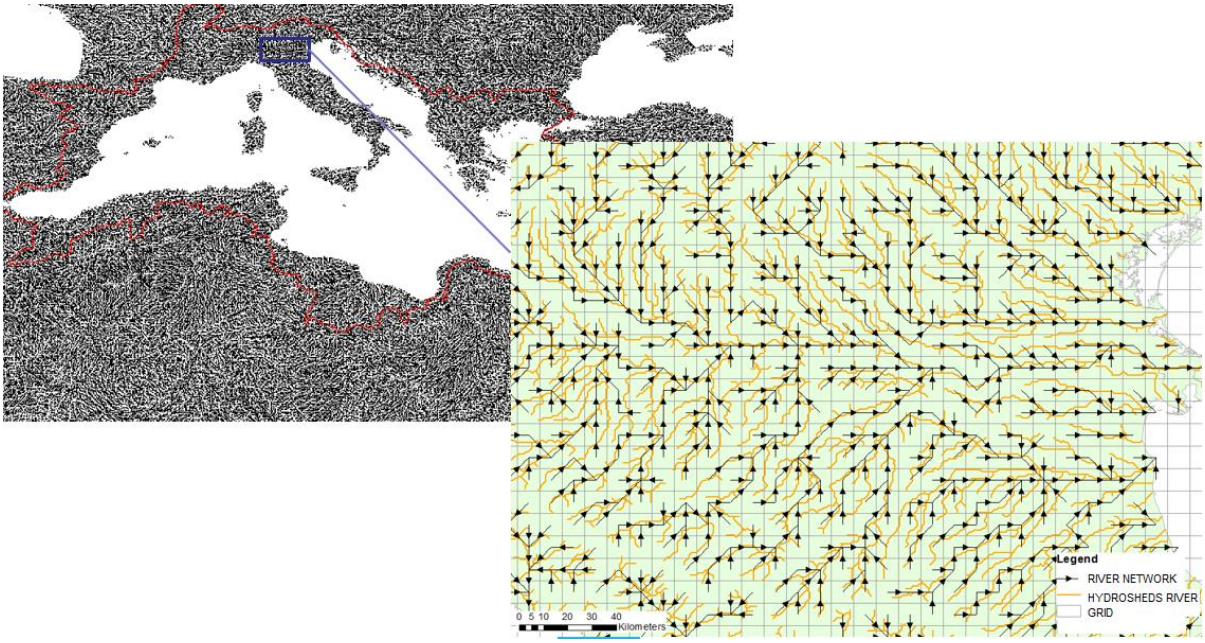

Figure 23. Mediterranean river network at 5-minutes and comparison with HydroSHEDS rivers.

4. Modelling results

4.1 Calibration and evaluation of model performance

The model was applied on all basins draining into the Mediterranean Sea (Figure 24). The GREEN-Rgrid model was calibrated for the year 2005 in 23 monitoring points mainly localized in the northern part of the Mediterranean area since in the southern part only very recent data (not covering year 2005) was available (Figure 24). The model was evaluated considering the whole dataset of points available for the year 2005.

As detailed previously we used a Latin hypercube sampling approach to run the model 100 times sampling the whole predefined range of α_P, α_R and α_N. The calibration of total nitrogen TN loads for year 2005 yielded satisfactory NSE (NSE=0.94) and the scatter plots of simulated and calibrated loads in terms of absolute loads (ton) and specific loads (ton/km^2) are shown in Figure 25. The plots show the good correlation with observation both for loads and specific loads also in the evaluation (we could not split the dataset in a calibration and validation subsets due to the very limited number of available monitoring points) as shown in Figure 26. The simulation with the highest NSE coefficient (0.94) yielded values for α_P, α_R and α_N of 4.72, 0.007, and 0.34, respectively.

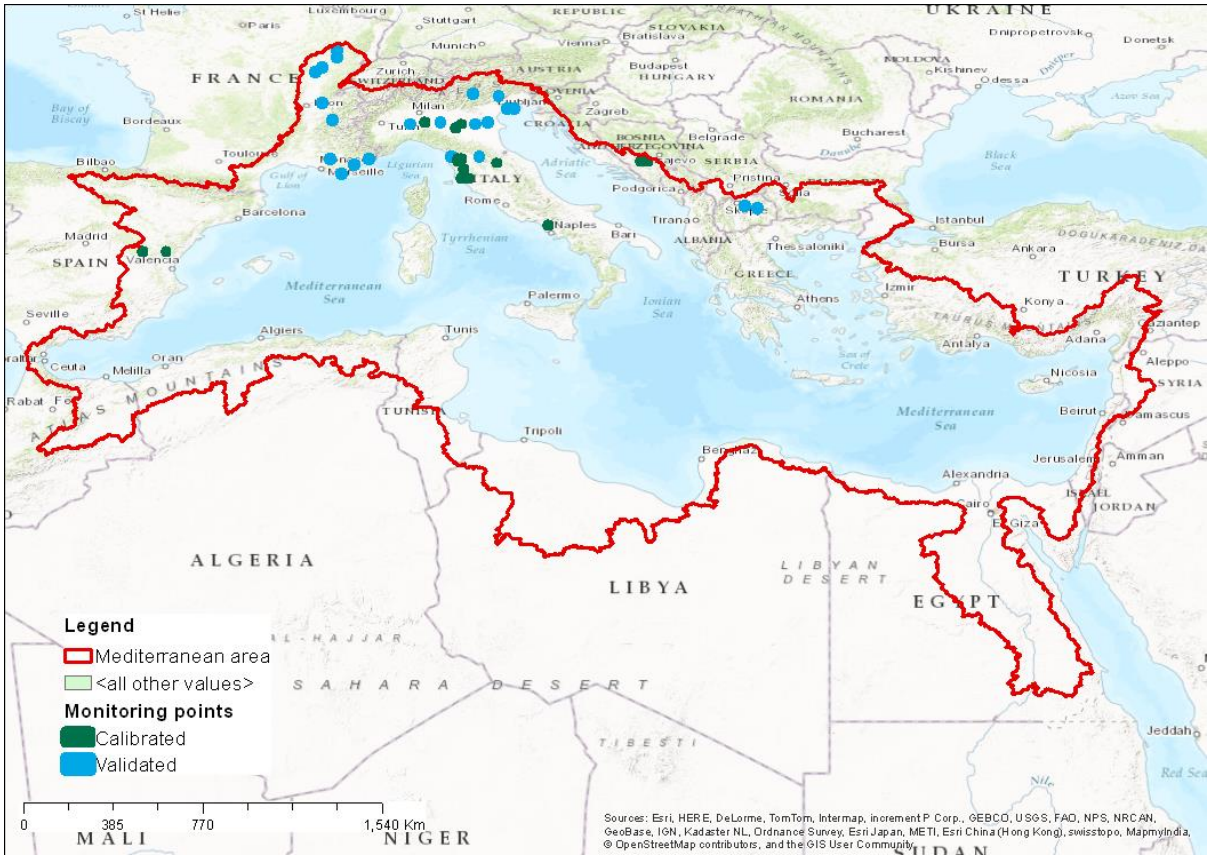

Figure 24. Spatial localization of monitoring points involved in the calibration (blue points) and in the evaluation (green points). The model evaluation was performed considering together the green and blue points.

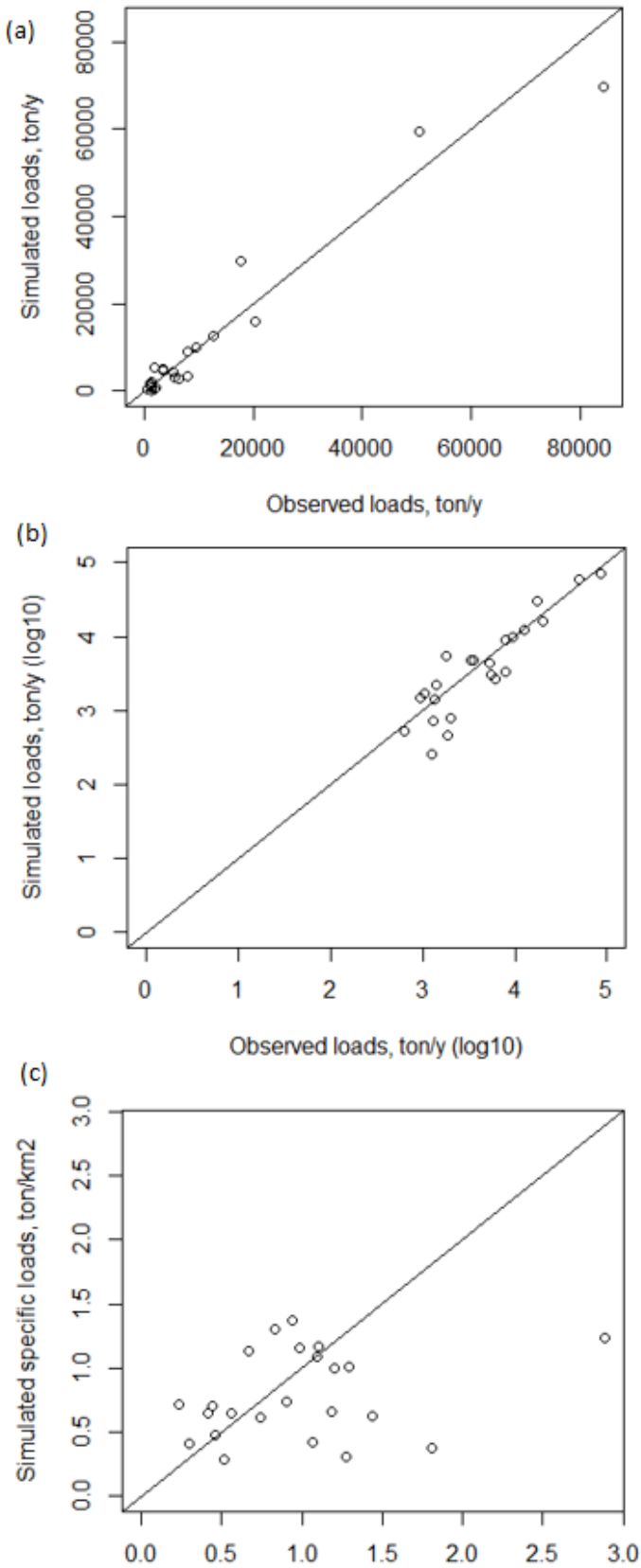

Figure 25. In (a) and (b): measured and estimated total nitrogen loads for year 2005 for 23 monitoring stations selected for the calibration. In (c) we display the comparison between measured and simulated specific loads

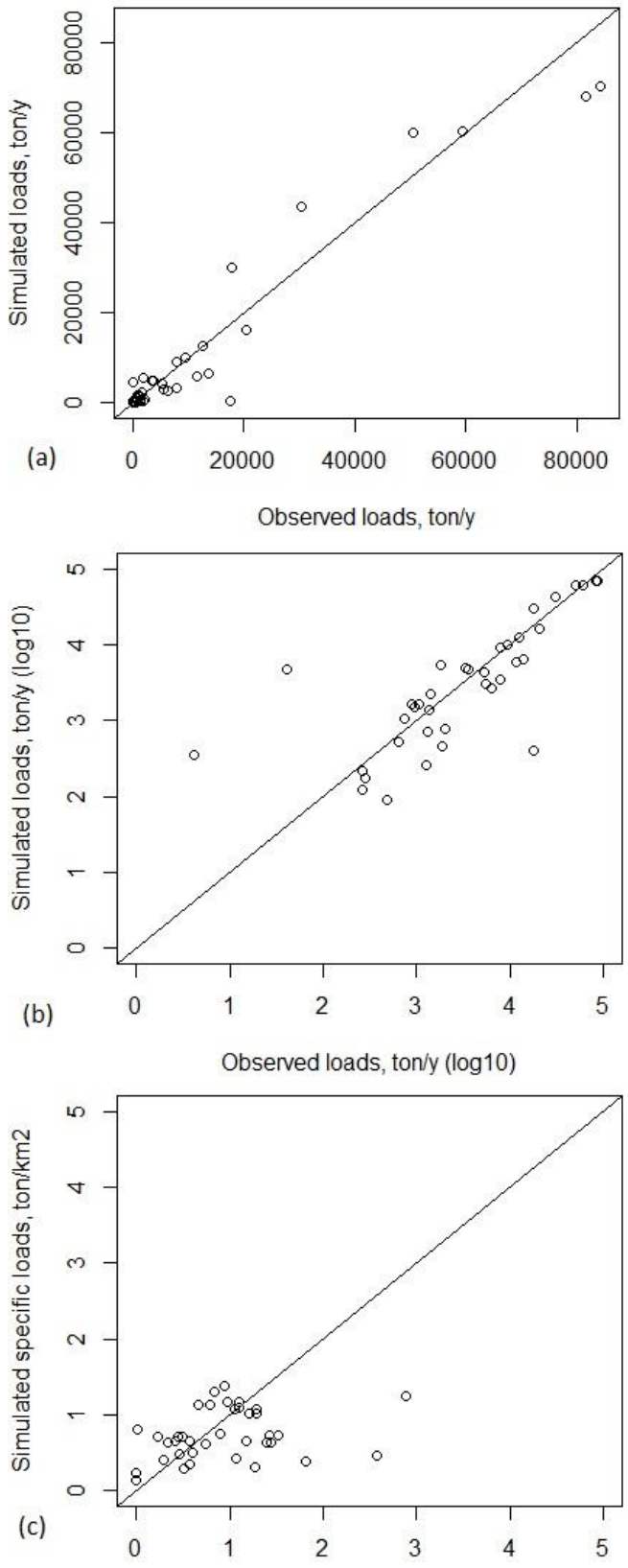

Figure 26. In (a) and (b): measured and estimated total nitrogen loads for year 2005 for the whole dataset (#38) of monitoring stations. In (c) we display the comparison between measured and simulated specific loads

4.2 Scenarios building

The model predicted an annual load of nitrogen into the Mediterranean Sea around 1.6 10^6 ton/yr that is completely in line with the 1.65 10^6 ton/yr for year 2000 reported by Strobl et al. (2009) and the 2.1 10^6 ton/yr reported by Beusen et al. (2016) for year 2000. The model, being satisfactorily calibrated, was used to investigate the impact of alternative management practices on TN emissions. Two scenarios were investigated and compared with the baseline (BASE):

- Surplus reduction (S1): the nitrogen surplus (when positive) was decreased of 50%.
- Improvement of WWTP treatment efficiency (S2) assuming that all treated wastewater underwent tertiary treatment (Table 4).

4.3 Results and discussion

The baseline (BASE) and the scenarios (S1 and S2) were compared in terms of total TN emission loads and specific loads.

Figure 27 shows the comparison between the simulated nutrient loads to Mediterranean Sea. It is noteworthy that TN loads to Mediterranean Sea resulted substantially reduced in S1 by about 28%, while in S2 the reduction of the load is only 9% with high associated costs (infrastructure, maintenance, etc.).

The interquartile range of TN loads was within the interval 7.5-122.5 ton/y for BASE and S2, whereas for S1 the values were within 4.5-82 (Figure 27), indicating that scenario S1 lead to a significant reduction of nitrogen emission on high intensity agricultural cells. Similar results were observed for the specific loads (Figure 28): the interquartile range of specific loads of BASE and S2 was within 0.05-1.8 ton/km^2, whereas for S1 the interquartile range was restricted to 0.04-0.5.

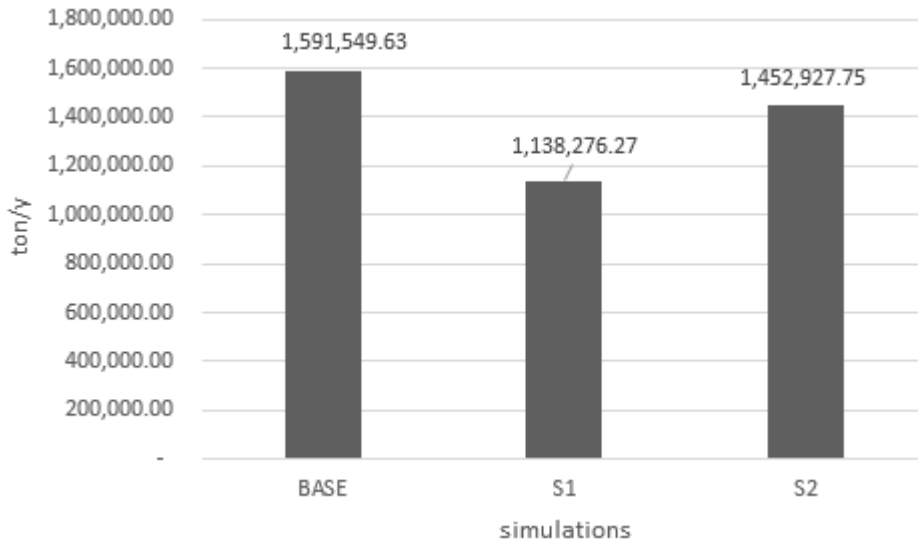

Figure 27. Comparison of total TN loads in the Mediterranean Sea between the three scenarios

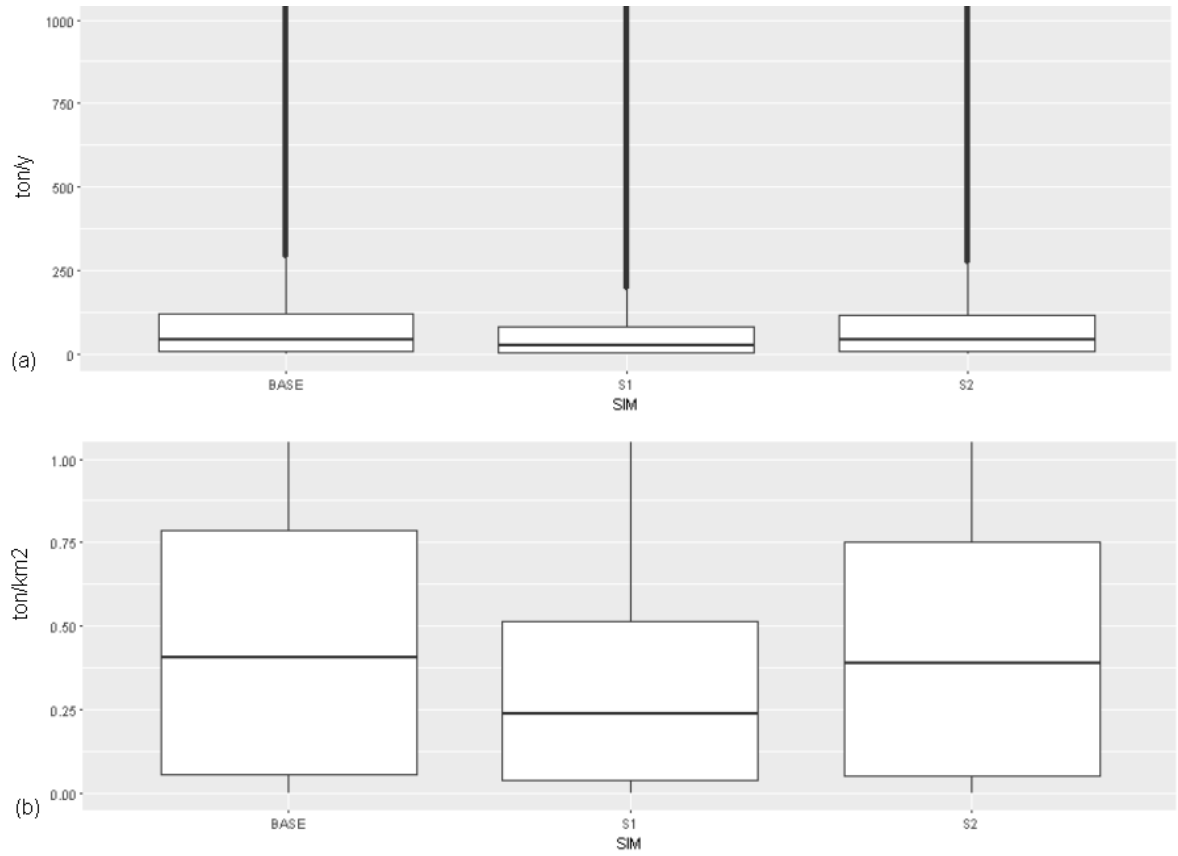

Figure 28 Comparison of total TN loads (a) and specific loads (b) in the Mediterranean basins

The following maps show the spatial distribution of loads and specific loads in the Mediterranean grid cells for BASE, S1, and S2 scenarios. The figures show that the effectiveness of agricultural scenario S1 is very high (Figure 30 and Figure 33) resulting in a substantial reduction of nutrient emissions in the Ebro and Rhone River Basins as well as in the Mediterranean basins of Algeria and Tunisia. Instead, the S2 scenario has lower effectiveness with respect to S1 resulting in a similar spatial distribution of loads and specific loads to that of the baseline.

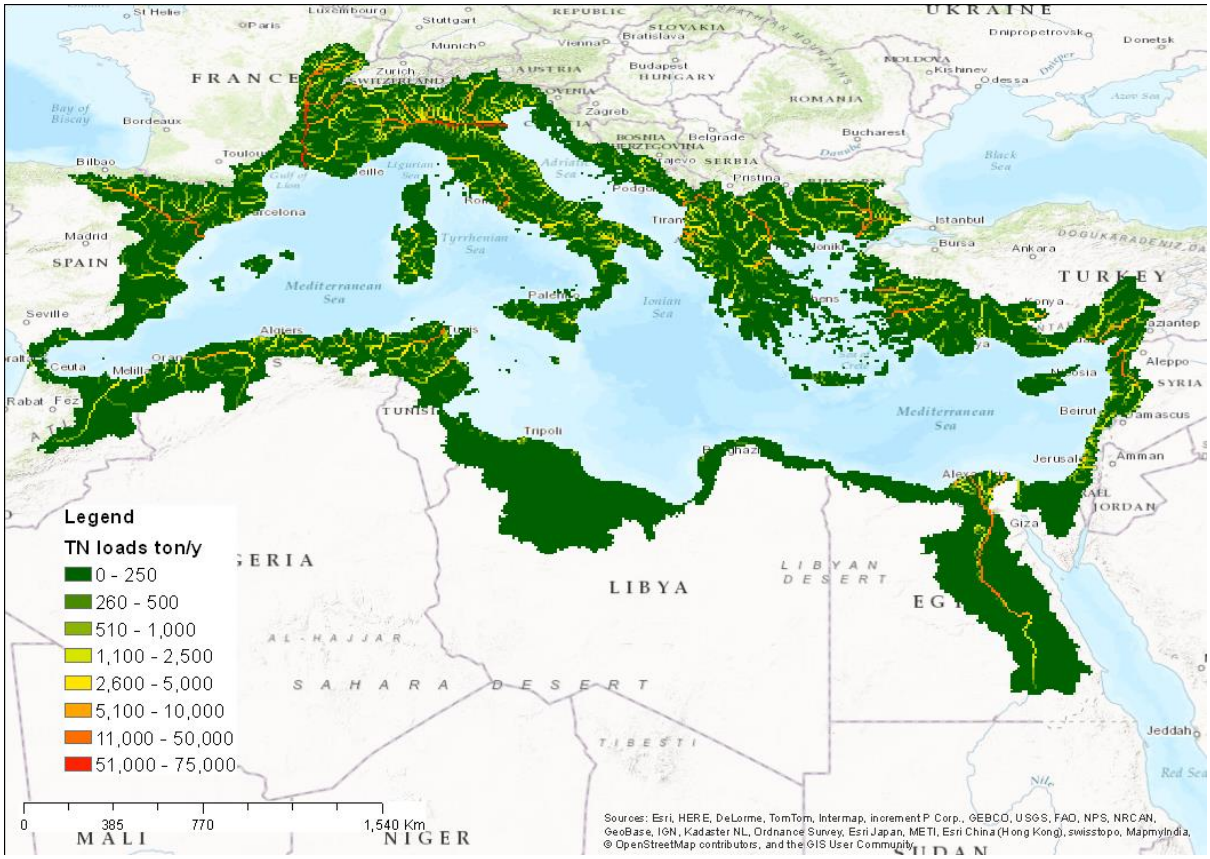

Figure 29 Raster map of total nitrogen loads per grid cell simulated under the baseline simulation (BASE)

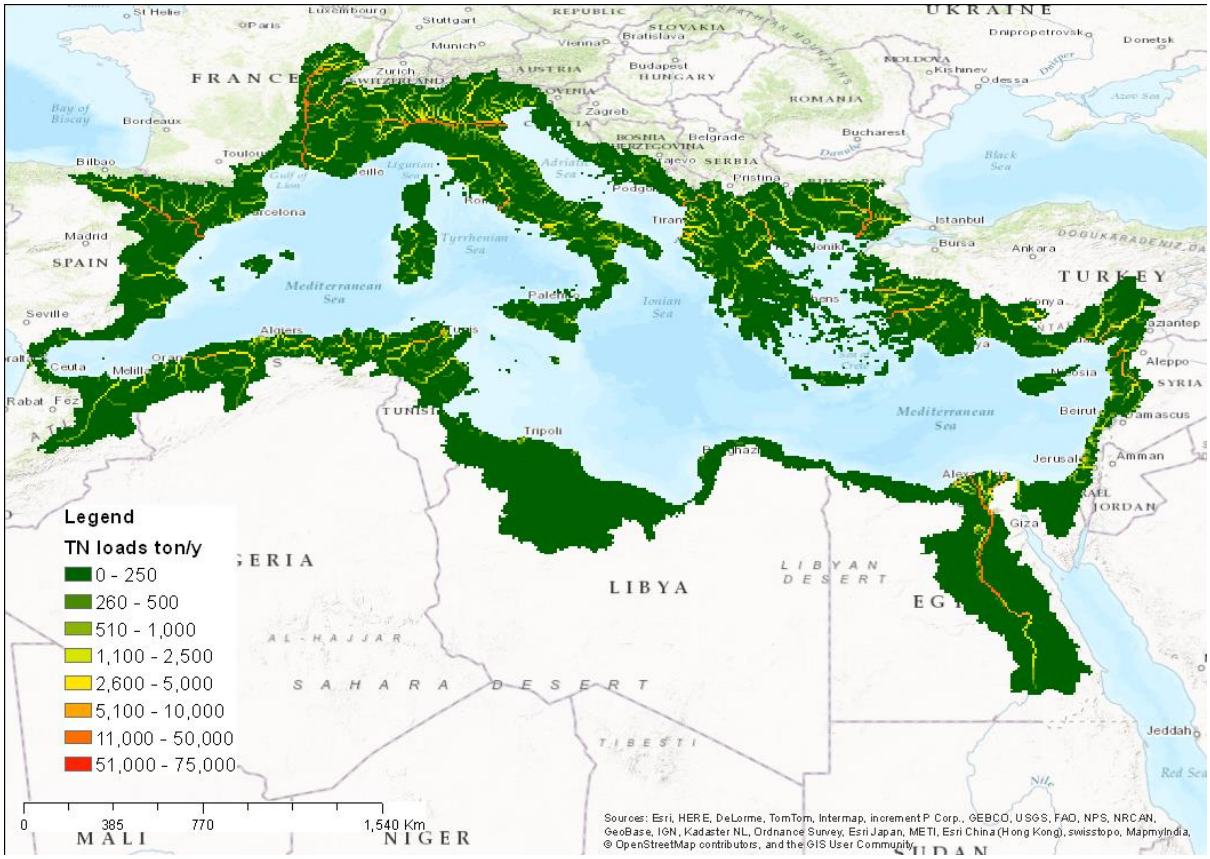

Figure 30. Raster map of total nitrogen loads per grid cell simulated under the scenario S1

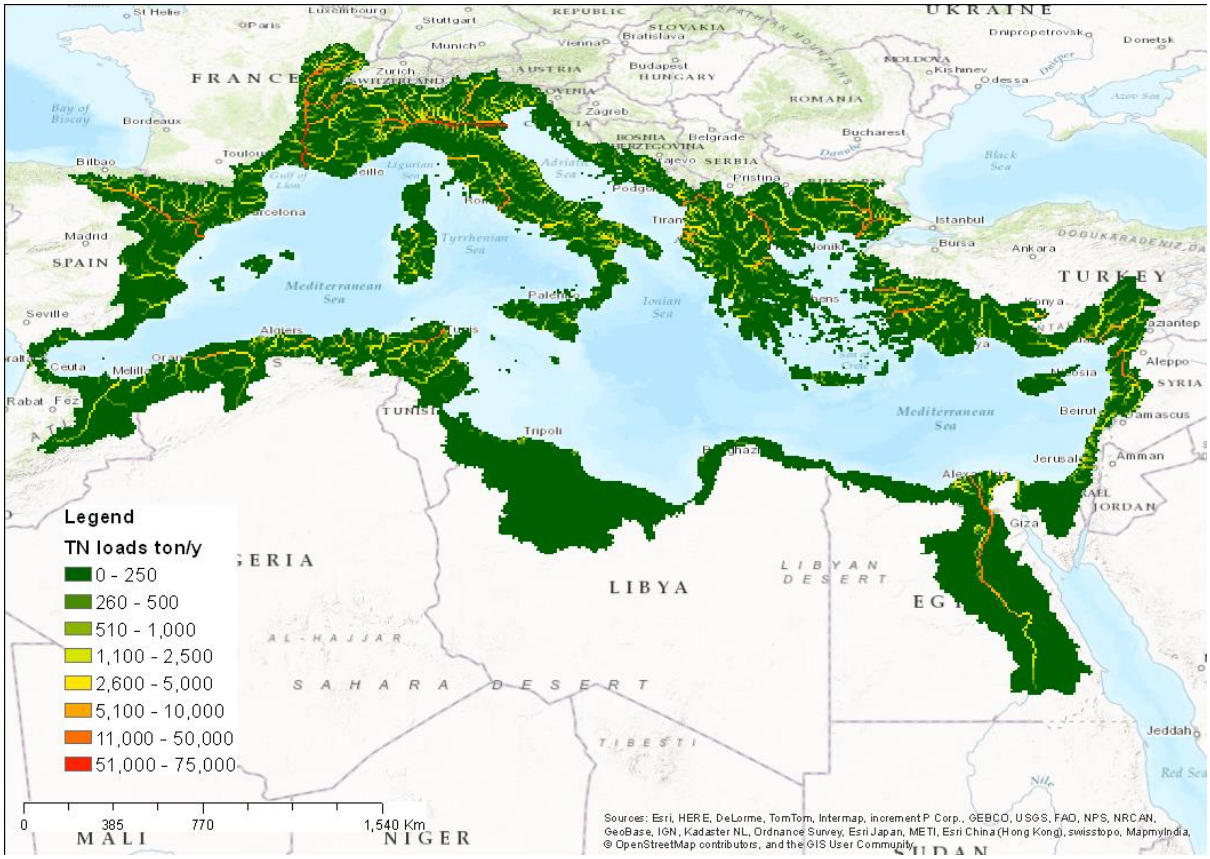

Figure 31. Raster map of total nitrogen loads per grid cell simulated under the scenario S2

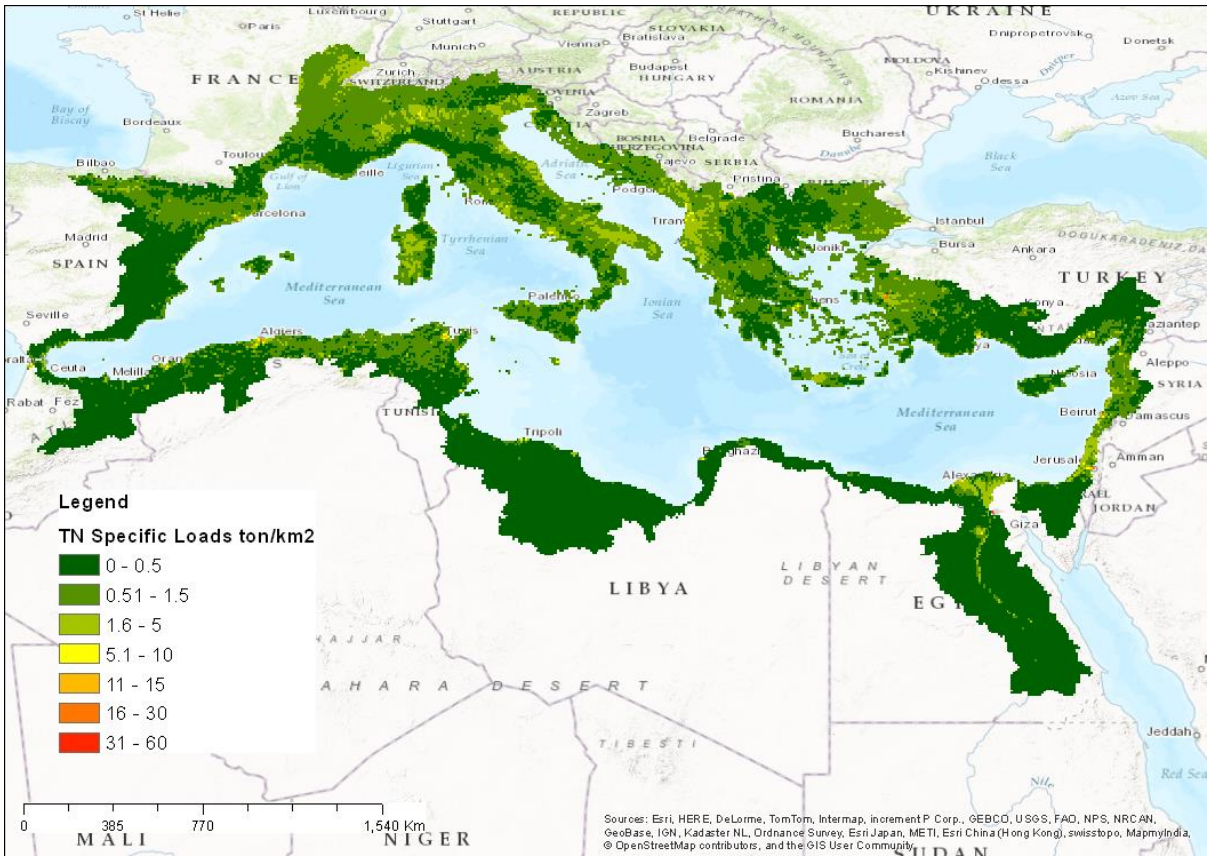

Figure 32 Raster map of total nitrogen specific loads per grid cell simulated under the baseline simulation (BASE)

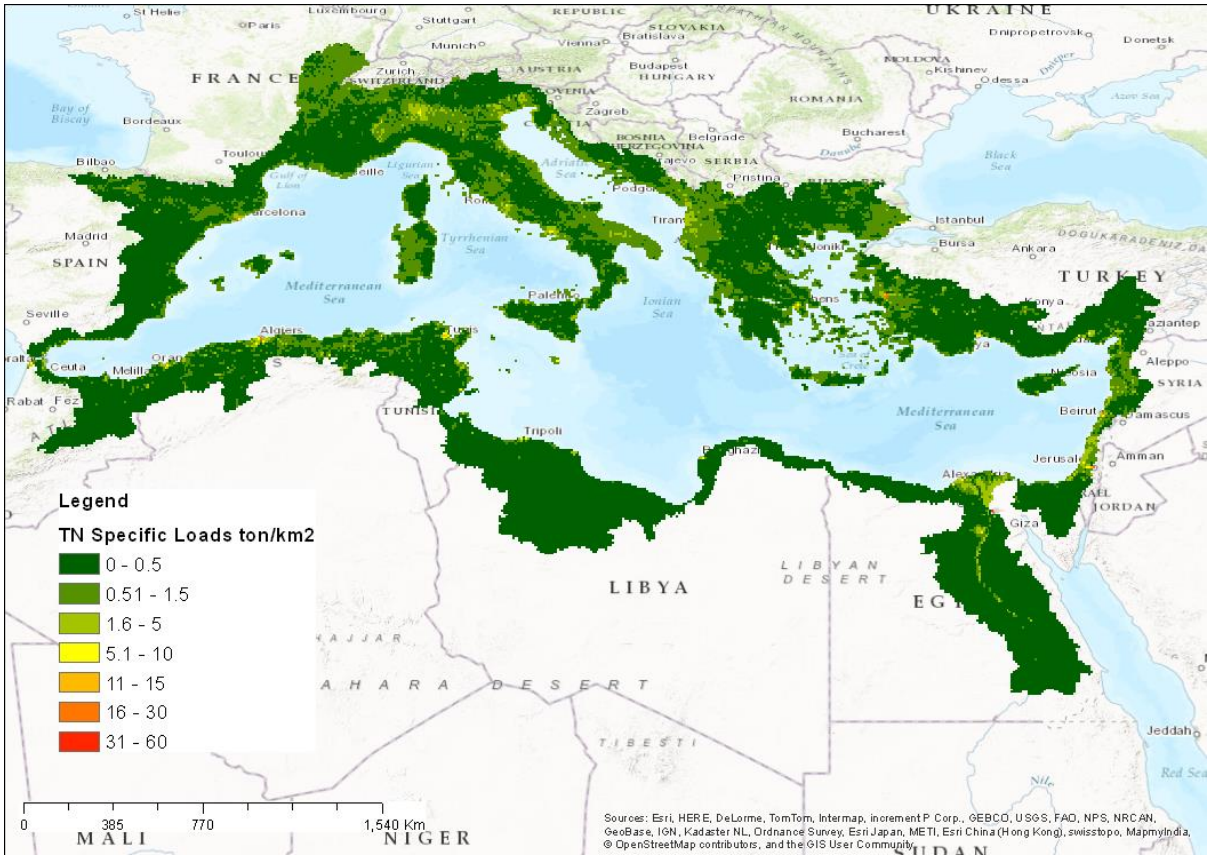

Figure 33. Raster map of total nitrogen specific loads per grid cell simulated under the scenario S1

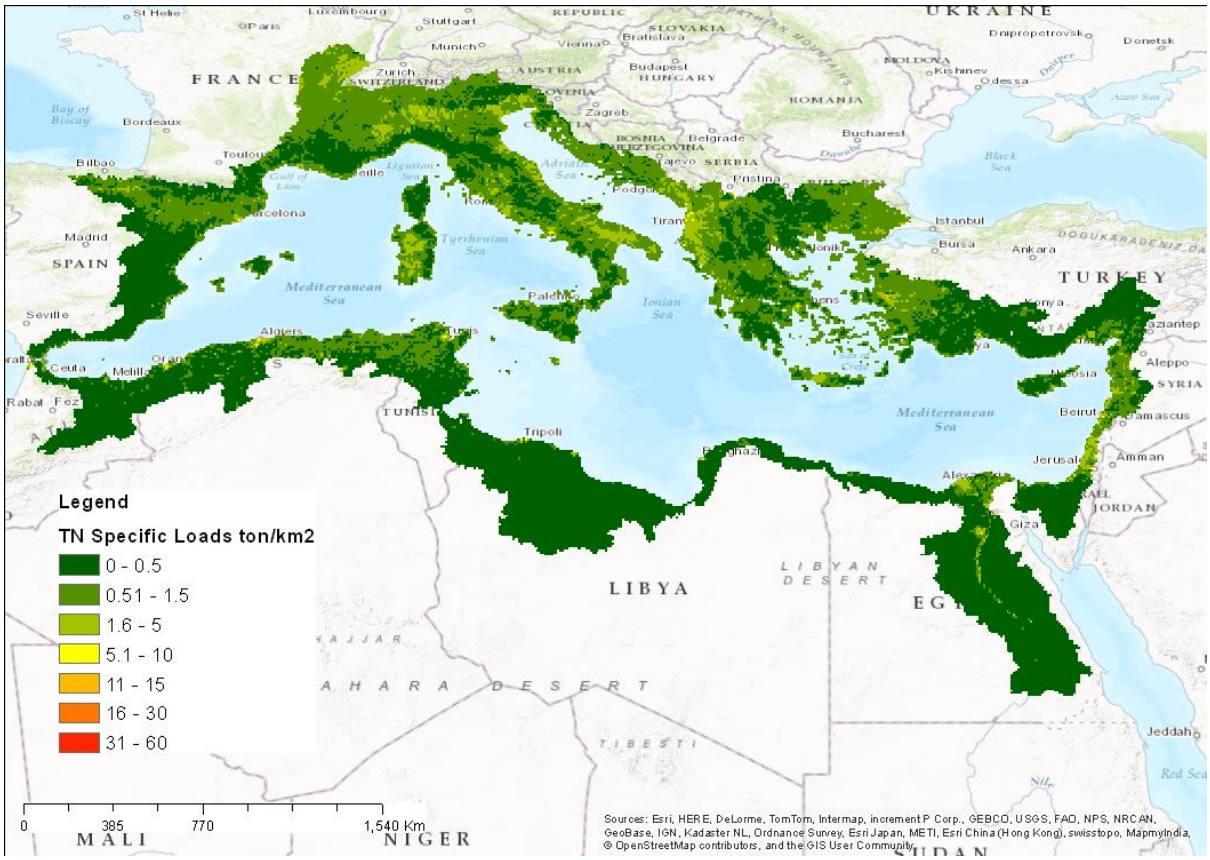

Figure 34. Raster map of total nitrogen specific loads per grid cell simulated under the scenario S2

5. Conclusions

In this study a new version of GREEN model (GREEN-Rgrid) was applied to simulate the nutrient loads entering the Mediterranean sea using a grid based approach at high spatial resoluion of 5-arc-minutes. The model was setup using the latest and best availllable data at global scale and it was calibrated and evaluated using annual loads for year 2005 respectivly in 23 and 38 monitoring points (entire dataset).

The calibration and validation analysis showed that the model was able to predict efficiently the TN loads and the specific loads in the Mediterranean area. The predicted total TN load entering into the sea was about 1.6 million of ton/y and it was comparable with other modelling predictions reported in literature (i.e. Ludwig et al., 2009; Strobl et al., 2009).
Two scenarios were then applied to identify the most effective option for reducing TN loads. The S1 scenario that consists in the reduction of surplus of 50% resulted in the most effective option for reducing the loads in the Mediterranean area and it was coherent with the MANU scenario provided in Thieu et al. (2012). The S2 scenario (increase of efficiency of treatment of WWTPs) was less significant and suggested a future deeper investigation related to the total phosphorus impact.

In conclusion, the GREEN-Rgrid model is a reliable tool for the prediction of nutrient loads at grid cell level making it a valuable tool for assessing different options for nutrient reduction from point and diffuse sources not only in the Mediterranean area but also globally.

6. References

Arino, O., Bicheron, P., Achard, F., Latham, J., Witt, R., and Weber, J. L., 2008. Globcover: the most detailed portrait of Earth, ESA Bulletin, 136, pp. 24-31.

Benoit, G., and A. Comeau (2005), A sustainable future for the Mediterranean, the Blue Plan's environment and development outlook, Earthscan, London, UK.

Beusen, A.H.W., Bouwman, A.F., Van Beek, L.P.H., Mogollón, J.M., Middelburg, J.J., 2016. Global riverine N and P transport to ocean increased during the 20th century despite increased retention along the aquatic continuum. Biogeosciences, 13 (8), pp. 2441-2451

Bouwman, A.F., Boumans, L.J.M., Batjes, N.H., 2002. Estimation of global NH 3 volatilization loss from synthetic fertilizers and animal manure applied to arable lands and grasslands. Global Biogeochemical Cycles 16 (2), 1024.

Bouwman, A.F., et al., 1997. A global high-resolution emission inventory for ammonia. Global Biogeochemical Cycles 11, 561–587.

Calloway, D. H., and S. Margen, 1971. Variation in endogenous nitrogen excretion and dietary nitrogen utilization as determinants of human protein requirement, J. Nutr., 101(2), 205–216.

Chen, M., Graedel, T.E., 2016. A half-century of global phosphorus flows, stocks, production, consumption, recycling, and environmental impacts. Global Environmental Change, 36, pp. 139-152.

Dijkstra L., and Poelmann H., 2014. A harmonised definition of cities and rural areas: the new degree of urbanization. European Commission Urban and Regional Policy. Working paper 1 (2014): 2014.

FAO, 2011. Global food losses and food waste – Extent, causes and prevention. Rome.

FAOSTAT, 2016. Food Supply - Crops Primary Equivalent. Available at http://www.fao.org/faostat/en/#data/CC/metadata.

Fuhrmeister, E.R., Schwab, K.J., Julian, T.R., 2015. Estimates of Nitrogen, Phosphorus, Biochemical Oxygen Demand, and Fecal Coliforms Entering the Environment Due to Inadequate Sanitation Treatment Technologies in 108 Low and Middle Income Countries. Environmental Science and Technology, 49 (19), pp. 11604-11611.

GeoNetwork available at http://www.fao.org/geonetwork/srv/en/main.home (accessed September 2016).

Grizzetti, B., Bouraoui, F., & De Marsily, G., 2008. Assessing nitrogen pressures on European surface water Glob. Biogeochem. Cycles, 22, GB4023.

Grizzetti, B., Bouraoui, F., Aloe, A., 2012. Changes of nitrogen and phosphorus loads to European seas. Global Change Biology, 18 (2), pp. 769-782.

International Fertilizer Industry Association (IFA) Statistics – IFADATA. 2011. Available at: http://www.fertilizer.org/ifa/Home-Page/STATISTICS (accessed September 2016).

Jönsson, H., Vinnerås, B., 2004. Adapting the nutrient content of urine and faeces in different countries using FAO and Swedish Data. Peer reviewed paper in the proceedings of the 2nd International Symposium on ecological sanitation, incorporating the 1st IWA specialist group conference on sustainable sanitation, Division 44, Environment and Infrastructure sector project ecosan; 7th–11th April, 2003, Lübeck, Germany. Published by GTZ, Postfach 5180, 65726 Eschborn, Germany.http://www.gtz.de.

Kundu, S., Vassanda Coumar, M., Rajendiran, S., Ajay, Subba Rao, A., 2015. Phosphates from detergents and eutrophication of surface water ecosystem in India. Current Science, 108 (7).

Lacirignola, C., Capone, R., Debs, P., El Bilali, H., & Bottalico, F., 2014. Natural Resources – Food Nexus: Food-Related Environmental Footprints in the Mediterranean Countries. Frontiers in Nutrition, 1, 23.

Lassaletta, L., Billen, G., Grizzetti, B., Anglade, J. & Garnier, J., 2014. 50 year trends in nitrogen use efficiency of world cropping systems: the relationship between yield and nitrogen input to cropland. Environ. Res. Lett. 9, 105011.

Lehner, B., Verdin, K., Jarvis, A., 2008.New global hydrography derived from spaceborne elevation data. Eos, Transactions, AGU, 89(10): 93-94.

Liu J., You L., Amini M., Obersteiner M., Herrero M., Zehnder A. J .B. and Yang H., 2010. A high-resolution assessment on global nitrogen flows in cropland Proc. Natl. Acad. Sci. USA 107 8035–40.

Liu, Y., Villalba, G., Ayres, R.U., Schroder, H., 2008. Global phosphorus flows and environmental impacts from a consumption perspective. Journal of Industrial Ecology, 12 (2), pp. 229-247.

Ludwig, W., Bouwman, A.F., Dumont, E., Lespinas, F., 2010. Water and nutrient fluxes from major Mediterranean and Black Sea rivers: Past and future trends and their implications for the basin-scale budgets. Global Biogeochemical Cycles, 24 (4).

Ludwig, W., Dumont, E., Meybeck, M., Heussner, S., 2009. River discharges of water and nutrients to the Mediterranean and Black Sea: Major drivers for ecosystem changes during past and future decades? Progress in Oceanography, 80 (3-4), pp. 199-217.

Milbrant, A., 2005. A Geographic Perspective on the Current Biomass Resource Availability in the United States (National Renewable Energy Laboratory, Golden, CO.

Morée, A.L., Beusen, A.H.W., Bouwman, A.F., Willems, W.J., 2013. Exploring global nitrogen and phosphorus flows in urban wastes during the twentieth century. Global Biogeochemical Cycles, 27 (3).

Nash, J. E. and Sutcliffe, J. V., 1970. River flow forecasting through conceptual models, Part I - A discussion of principles, J. Hydrol., 10, 282–290, 1970.

Neitsch, S. L., Arnold, J. G., Kiniry, J. R., Srinivasan, R., and Williams, J. R., 2010. Soil and Water Assessment Tool Input/Output File Documentation Version 2009, Grassland, Soil and Water Research Laboratory, Agricultural Research Service and Blackland Research Center, Texas Agricultural Experiment Station, College Station, Texas.

Olivera, F., Lear, M. S., Famiglietti, J. S. & Asante, K., 2002. Extracting low-resolution river networks from high resolution digital elevation models. Water Resour. Res. 38(11), 1231–1239.

Oron, G., 2003. Agriculture, water and the environment: future challenges, Water Sci. Technol. Water Supply, 3(4), 51-57.

Pebesma, E.J., R.S. Bivand, 2005. Classes and methods for spatial data in R. R News 5 (2), https://cran.r-project.org/doc/Rnews/.

Riddick, S. and Ward, D. and Hess, P. and Mahowald, N. and Massad, R. and Holland, E., 2016. Estimate of changes in agricultural terrestrial nitrogen pathways and ammonia emissions from 1850 to present in the Community Earth System Model. Biogeosciences, 13, 3397–3426, 2016

Roger S. Bivand, Edzer Pebesma and Virgilio Gomez-Rubio, 2013. Applied spatial data analysis with R, Second edition. Springer, NY. http://www.asdar-book.org/

Sheldrick W., Keith Syers J., Lingard J., 2003. Contribution of livestock excreta to nutrient balances. Nutr Cycl Agroecosys 66:119 –131.

Soetaert, K., and Petzoldt, T., 2010. Inverse modelling, sensitivity and Monte Carlo analysis in R using package FME. Journal of Statistical Software, 33(3):1–28.

Strobl, R.O., Somma, F., Evans, B.M., Zaldívar, J.M., 2009. Fluxes of water and nutrients from river runoff to the Mediterranean Sea using GIS and a watershed model. Journal of Geophysical Research: Biogeosciences, 114 (3).

Thieu, V., Bouraoui, F., Aloe, A., and Bidoglio, G., 2012. Scenario analysis of pollutants loads to European regional seas for the year 2020: I. Policy options and alternative measures to mitigate land based emission of nutrients EC-JRC Report (Luxembourg) 83.

Vet, R., Artz, R.S., Carou, S., Shaw, M., Ro, C.-U., Aas, W., Baker, A., Bowersox, V.C., Dentener, F., Galy-Lacaux, C., Hou, A., Pienaar, J.J., Gillett, R., Forti, M.C., Gromov, S., Hara, H., Khodzher, T., Mahowald, N.M., Nickovic, S., Rao, P.S.P., Reid, N.W., 2014. A global assessment of precipitation chemistry and deposition of sulfur, nitrogen, sea salt, base cations, organic acids, acidity and pH, and phosphorus. Atmospheric Environment, 93, pp. 3-100.

WHO, 2016. Available at http://www.who.int/water_sanitation_health/monitoring/jmpfinal.pdf.

Williams, J.R., 1995. The EPIC model. In: Computer models of watershed hydrology editors Singh, V.P. Water Resources Publications, Highlands Ranch, CO, USA, pp. 909-1000.

World Bank. 2008. The Sanitation, Hygiene and Wastewater Resource Guide.

You, L., Wood,S., Wood-Sichra, U., Wu, W., 2014. Generating global crop distribution maps: From census to grid, Agricultural Systems, Volume 127, Pages 53-60.

List of figures

Figure 1. Global spatial distribution of arable land extent (km^2) at 5 minutes grid cell resolution. 10

Figure 2. Global spatial distribution of forest extent (km^2) at 5 minutes grid cell resolution. 11

Figure 3. Global spatial distribution of grass land (km^2) at 5 minutes grid cell resolution. 11

Figure 4. Global spatial distribution of crop nitrogen uptake for wheat (kg/ha) 14

Figure 5. Global spatial distribution of nitrogen residue of soybean (kg/ha) 14

Figure 6. Global spatial distribution of total nitrogen fixation (kg/ha) 15

Figure 7. Global spatial distribution of TN mineral fertilizers applied (kg/ha) 16

Figure 8. Global spatial distribution of TP mineral fertilizers (kg/ha) 17

Figure 9. Global spatial distribution of TN manure fertilizers (kg/ha). 19

Figure 10. Global spatial distribution of TP manure fertilizers (kg/ha) 19

Figure 11. Flow chart for the calculation of points sources and scattered dwellings. 21

Figure 12. STP-detergent versus GDP per capita in 2005. 23

Figure 13. Global spatial distribution of urban connected population 24

Figure 14. Global spatial distribution of rural connected population 25

Figure 15. Global spatial distribution of N emission (ton/y) from urban connected population 25

Figure 16. Spatial distribution of N emission (ton/y) from urban connected population (focus Mediterranean area) 26

Figure 17. Global spatial distribution of N emission (ton/y) from rural connected population 26

Figure 18. Spatial distribution of N emission (ton/y) from rural connected population (focus Mediterranean area) 27

Figure 19. Global spatial distribution of N emission (ton/y) from total unconnected population ("improved" category) 27

Figure 20. Spatial distribution of N emission (ton/y) from total unconnected population ("improved" category) (focus Mediterranean area) 28

Figure 21. Global spatial distribution of nitrogen deposition (kg/ha) 29

Figure 22. Comparison between the drainage area of basins in Europe obtained from the new river network at 5-minutes and HydroSHEDS Basins. 30

Figure 23. Mediterranean river network at 5-minutes and comparison with HydroSHEDS rivers. 31

Figure 24. Spatial localization of monitoring points involved in the calibration (blue points) and in the evaluation (green points). The model evaluation was performed considering together the green and blue points. 32

Figure 25. In (a) and (b): measured and estimated total nitrogen loads for year 2005 for 23 monitoring stations selected for the calibration. In (c) we display the comparison between measured and simulated specific loads 33

Figure 26. In (a) and (b): measured and estimated total nitrogen loads for year 2005 for the whole dataset (#38) of monitoring stations. In (c) we display the comparison between measured and simulated specific loads 34

Figure 27. Comparison of total TN loads in the Mediterranean Sea between the three scenarios 35

Figure 28 Comparison of total TN loads (a) and specific loads (b) in the Mediterranean basins..... 36

Figure 29 Raster map of total nitrogen loads per grid cell simulated under the baseline simulation (BASE) 37

Figure 30. Raster map of total nitrogen loads per grid cell simulated under the scenario S1..... 37

Figure 31. Raster map of total nitrogen loads per grid cell simulated under the scenario S2..... 38

Figure 32 Raster map of total nitrogen specific loads per grid cell simulated under the baseline simulation (BASE)..... 38

Figure 33. Raster map of total nitrogen specific loads per grid cell simulated under the scenario S1 39

Figure 34. Raster map of total nitrogen specific loads per grid cell simulated under the scenario S2 39

List of tables

Table 1. SPAM crops and related coefficients used in this work. 13

Table 2. Percentage of food waste according to different geographical regions (FAO, 2011) 20

Table 3. Connection and treatment level for Europe and OECD countries 22

Table 4. Nutrient and BOD removal efficiency for the various sanitation and treatment types 22

Table 5. Summary of Global emission source for nitrogen and phosphorus 23

Europe Direct is a service to help you find answers to your questions about the European Union.

Freephone number (*)**:**

00 800 6 7 8 9 10 11

(*) The information given is free, as are most calls (though some operators, phone boxes or hotels may charge you).

More information on the European Union is available on the internet (http://europa.eu).

HOW TO OBTAIN EU PUBLICATIONS

Free publications:

- one copy:
  via EU Bookshop (http://bookshop.europa.eu);
- more than one copy or posters/maps:
  from the European Union's representations (http://ec.europa.eu/represent_en.htm);
  from the delegations in non-EU countries (http://eeas.europa.eu/delegations/index_en.htm);
  by contacting the Europe Direct service (http://europa.eu/europedirect/index_en.htm) or
  calling 00 800 6 7 8 9 10 11 (freephone number from anywhere in the EU) (*).

  (*) The information given is free, as are most calls (though some operators, phone boxes or hotels may charge you).

Priced publications:

- via EU Bookshop (http://bookshop.europa.eu).

KJ-NA-28424-EN-N

JRC Mission

As the science and knowledge service of the European Commission, the Joint Research Centre's mission is to support EU policies with independent evidence throughout the whole policy cycle.

EU Science Hub
ec.europa.eu/jrc

@EU_ScienceHub

EU Science Hub - Joint Research Centre

Joint Research Centre

EU Science Hub

Publications Office

doi:10.2760/51281

ISBN 978-92-79-65145-8